"I never satisfy myself until I can make a mechanical model of a thing. If I can make a mechanical model I can understand it. As long as I cannot make a mechanical model all the way through I cannot understand; and that is why I cannot get the electromagnetic theory ..... But I want to understand light as well as I can, without introducing things that we understand even less of. That is why I take plain dynamics. I can get a model in plain dynamics; I cannot in electromagnetics."

LORD KELVIN, BALTIMORE LECTURES, 1904

4

Smoothed Particle Magnetohydrodynamics

4.1 Introduction

Given the suitability of SPH for studies of star formation, it is unsurprising that magnetic field effects, which are known to be important or even crucial in the star formation process, were incorporated into SPH from the outset (Gingold and Monaghan, 1977). The application in this case was to static magnetic polytropes where good agreement was found between the SPH solution and perturbation calculations. Dynamical problems were considered by Phillips (1983b) and applied to star formation problems (Phillips, 1982, 1983a, 1985, 1986a,b; Benz, 1984; Phillips and Monaghan, 1985). In the latter it was shown that when the conservation form of the equations was used an instability developed which took the form of SPH particles clumping. SPH blast waves in a magnetic medium were studied by Stellingwerf and Peterkin (1990, 1994). Habe et al. (1991), Murray et al. (1996) and Mac Low et al. (1999) used a form of the SPH equations where the magnetic fields were updated on a grid and interpolated to the SPH particles.

Meglicki (1994, 1995) and Meglicki et al. (1995) used a formulation of 'Smoothed Particle Magnetohydrodynamics' (SPMHD) that uses a non-conservative ($\mathbf{J} \times \mathbf{B}$) force, which is always stable and guarantees that the magnetic force is exactly perpendicular to the magnetic field. This formalism was also used by Byleveld and Pongracic (1996) and more recently by Cerqueira and de Gouveia Dal Pino (2001, and references therein) and Hosking (2002), however the non-conservation of momentum leads to poor performance on shock-type problems. A conservative form of SPMHD has been used by Dolag et al. (1999) and by Marinho et al. (2001) since the magnetic field in their simulations remained in the regime where the instability does not appear. Morris (1996) suggested using a compromise between the conservative (tensor) force and the $\mathbf{J} \times \mathbf{B}$ formalism. Non-ideal MHD terms in SPH were also considered by Morris (1996), who suggested using resistive terms to control the divergence of the magnetic field and by Hosking and Whitworth (2004), who considered the effects of ambipolar diffusion via a two-fluid

model. The simulation of MHD shocks with SPH has been investigated by Børve (2001) (see Børve et al. 2001), where excellent results were obtained by periodically invoking a regularization procedure on the SPH particle distribution and by explicitly subtracting the effect of any non-zero divergence from the conservative formalism.

However, the simplicity with which the MHD equations can be written down belies the fact that there are a number of technical difficulties involved in their solution, which have not been fully addressed in an SPH context. The first technical difficulty with MHD simulations is that the magnetic field comes with the constraint $\nabla \cdot \mathbf{B} = 0$. As a first level treatment in this chapter, we follow the approach of Janhunen (2000) in formulating the MHD equations from the premise that non zero $\nabla \cdot \mathbf{B}$ terms may be generated but that a consistent treatment of such terms by the numerical method will reduce the error associated with their presence. Consistency is ensured in this case by deriving the SPMHD equations from a variational principle, using the discrete forms of the continuity and induction equations to constrain the discrete formulations of the momentum and energy equations. Further discussion of this and other approaches to maintaining the divergence constraint in an SPH context is deferred to Chapter 5.

A further technical difficulty peculiar to SPH is that when a conservative force is used the SPH particles tend to clump in pairs in the presence of tension. This was first noticed by Phillips and Monaghan (1985) and re-discovered by researchers applying SPH to elastic fracture problems (see the references in Monaghan 2000). Several remedies have been proposed (e.g. Dyka et al. 1997; Bonet and Kulasegaram 2000, 2001) but they all either involve a significant increase in computational expense or cannot be applied where the particle configuration changes significantly. The nature of this instability was systematically investigated in an MHD context by Morris (1996), with several solutions proposed. A further remedy for the tensile instability which can be easily applied to astrophysical problems has been recently proposed by Monaghan (2000). The idea is to add a small artificial stress which prevents particles from clumping in the presence of a negative stress. This term has been shown to work well in elastic dynamics simulations (Gray et al., 2001) and we apply it here to the MHD case.

The third technical difficulty is that shocks in MHD are much more complex than their hydrodynamic counterparts. This is due to the additional wave types which can result in a wide range of discontinuous structures, each of which must be treated appropriately by the numerical method. We approach this problem by formulating artificial dissipation terms appropriate to the MHD case (the major difference to the hydrodynamic case being the introduction of artificial resistivity at discontinuities in the magnetic field). These dissipative terms are derived in such a manner that the contribution to the entropy and thermal energy from viscosity, thermal conductivity and ohmic resistivity is guaranteed to be positive definite.

The chapter is organised as follows: In §4.2 we give the continuum form of the MHD equations and in §4.3 the SPH form of these equations, deriving the SPMHD equations self-consistently from a variational principle (§4.3.2). Consistent alternative formulations, similar to those derived in the SPH case (§3.4) are discussed in §4.3.4 whilst older formulations are also reviewed (§4.3.5). In §4.3.6 a variational principle is again used to extend the SPMHD equations to the case where the smoothing length is regarded as a function of local particle density. Stability considerations are discussed in §4.4 with the implementation of the instability correction of Monaghan (2000) presented in §4.4.1 as well as several alternative methods. Dissipation terms appropriate for MHD shocks analogous to those derived in the SPH case (§3.5) are given in §4.5. Finally, in §4.6 we present the results of extensive numerical tests

for one dimensional problems including a range of shock tube problems (§4.6.3), linear waves (§4.6.4) and magnetic Toy Stars (§4.6.5). The extension of the method to multidimensional problems is presented in Chapter 5.

4.2 Magnetohydrodynamics

Magnetohydrodynamics (MHD) is a one-fluid approximation to the equations of plasma physics, where the effects of static electric charge are assumed to be negligible and the non-relativistic limit is generally taken (relativistic MHD involves dropping the latter assumption, whilst retaining the former). The derivation of the MHD equations is given in many standard textbooks and we simply state the results here.

4.2.1 Continuum equations

The continuity equation for the density remains the same as in the non-magnetic case, ie.

$$\frac{d\rho}{dt} + \rho \nabla \cdot \mathbf{v} = 0, \tag{4.1}$$

implying the conservation of mass. The acceleration equation in the absence of dissipation may be expressed in conservative form as the gradient of a symmetric tensor, that is

$$\frac{d\mathrm{v}^i}{dt} = \frac{1}{\rho}\frac{\partial S^{ij}}{\partial x^j}, \tag{4.2}$$

where the stress S^{ij} in the case of ideal MHD is defined by

$$S^{ij} = -P\delta^{ij} + \frac{1}{\mu_0}\left(B^i B^j - \frac{1}{2}B^2\delta^{ij}\right). \tag{4.3}$$

where B^i is the ith component of the magnetic field and μ_0 is the permittivity of free space. In SI units $\mu_0 = 4\pi/10^7$. From the tensor formulation the magnetic force is easily interpreted in terms of an isotropic force due to gradients in the magnetic pressure and an anisotropic (tension) force resisting motion which is perpendicular to magnetic field lines. In vector notation (4.2) is given by

$$\frac{d\mathbf{v}}{dt} = -\frac{\nabla P}{\rho} + \frac{\mathbf{J}\times\mathbf{B}}{\rho} + \frac{\mathbf{B}\nabla\cdot\mathbf{B}}{\mu_0\rho}, \tag{4.4}$$

where $\mathbf{J} = \nabla\times\mathbf{B}/\mu_0$ is the magnetic current density. Under the assumption of $\nabla\cdot\mathbf{B} = 0$ (ie. no magnetic monopoles), the force becomes

$$\frac{d\mathbf{v}}{dt} = -\frac{\nabla P}{\rho} + \frac{\mathbf{J}\times\mathbf{B}}{\rho}. \tag{4.5}$$

The assumption of zero magnetic divergence is valid in the continuum case (making (4.4) and (4.5) equivalent) but requires careful consideration in a numerical context since the divergence is not guaranteed to be zero exactly. Discrete formulations based on the conservative form (4.4) can be made to conserve momentum exactly, whilst formulations based on the non-conservative form (4.5) can be made

to guarantee that the magnetic force is exactly perpendicular to the magnetic field. We use (4.4) since exact conservation of momentum is required in order to accurately simulate shocks, although older formalisms based on (4.5) are discussed in §4.3.5. The momentum conserving formulation (4.4) results naturally in the derivation of the SPMHD equations from a variational principle given in §4.3.2.

The equation for the update of the magnetic field is the induction equation. The standard form is derived from Maxwell's equations neglecting displacement currents and a generalised form of Ohm's law. We follow Janhunen (2000) and Dellar (2001) in formulating the induction equations so that it is consistent even if $\nabla \cdot \mathbf{B}$ does not vanish. The induction equation then takes the form

$$\frac{\partial \mathbf{B}}{\partial t} + \nabla \times (\mathbf{v} \times \mathbf{B}) = -\nabla \times (\eta \mathbf{J}) - \mathbf{v}(\nabla \cdot \mathbf{B}), \tag{4.6}$$

where the last term is the monopole current (Janhunen, 2000; Dellar, 2001) and η is the magnetic diffusivity $1/(\sigma\mu_0)$ where σ is the conductivity. Ideal MHD corresponds to the limit of infinite conductivity $\eta = 0$. Using the Lagrangian time derivative (4.6) can be written as

$$\frac{d\mathbf{B}}{dt} = -\mathbf{B}(\nabla \cdot \mathbf{v}) + (\mathbf{B} \cdot \nabla)\mathbf{v} - \nabla \times (\eta \mathbf{J}). \tag{4.7}$$

Taking the divergence of this equation, we find that monopoles evolve according to

$$\frac{\partial}{\partial t}(\nabla \cdot \mathbf{B}) + \nabla \cdot (\mathbf{v} \nabla \cdot \mathbf{B}) = 0, \tag{4.8}$$

which has the same form as the continuity equation for the density and therefore implies that the total volume integral of $\nabla \cdot \mathbf{B}$ is conserved (and therefore that the total *surface* integral of the magnetic flux is conserved which is the important physical quantity, rather than the *volume* integral which is conserved when the induction equation is written in a so-called 'conservative' form). Note also that in this form the induction equation can be written as

$$\frac{d}{dt}\left(\frac{\mathbf{B}}{\rho}\right) = \left(\frac{\mathbf{B}}{\rho} \cdot \nabla\right)\mathbf{v} - \frac{\nabla \times (\eta \mathbf{J})}{\rho}, \tag{4.9}$$

which demonstrates that in ideal MHD the flux per unit mass, $\mathbf{B}/\rho$ is passively advected by the flow and therefore that the magnetic field lines remain 'frozen' into the fluid.

The total energy per unit mass is given by

$$e = \frac{1}{2}\mathrm{v}^2 + u + \frac{B^2}{2\mu_0\rho}, \tag{4.10}$$

where u is the thermal energy per unit mass. The total energy e evolves according to

$$\frac{de}{dt} = \frac{1}{\rho}\frac{\partial (S^{ij}\mathrm{v}^j)}{\partial x^j} + \frac{1}{\rho}\nabla \cdot [\mathbf{B} \times (\eta \mathbf{J})]. \tag{4.11}$$

Alternatively the thermal energy equation can be used, which may be derived either from (4.10) giving

$$\frac{du}{dt} = \frac{de}{dt} - \mathbf{v} \cdot \frac{d\mathbf{v}}{dt} - \frac{d}{dt}\left(\frac{B^2}{2\mu_0\rho}\right), \tag{4.12}$$

or using the first law of thermodynamics. Either way, the resulting equation is given by

$$\frac{du}{dt} = -\frac{P}{\rho}\nabla \cdot \mathbf{v}, \tag{4.13}$$

which is the same as in the hydrodynamic case. The equation set is closed by an appropriate equation of state, which for a perfect gas is given by

$$P = (\gamma - 1)\rho u. \tag{4.14}$$

4.2.2 Conserved quantities

In order to monitor the quality of a simulation, it is useful to be able to measure the accuracy to which the algorithm conserves integrals of the motion. Aside from the usual conserved quantities of mass, momentum, angular momentum, energy and centre of mass, several additional quantities can be measured in MHD. A list of such quantities can be derived using Hamiltonian techniques and is given by (e.g.) Morrison and Hazeltine (1984). The helicity,

$$\int (\mathbf{A} \cdot \mathbf{B}) \mathrm{dV}, \tag{4.15}$$

where $\mathbf{B} = \nabla \times \mathbf{A}$, is a measure of the linkage of magnetic field lines (expressing the fact that magnetic field lines which are initially linked cannot become unlinked in the absence of dissipative terms). This quantity can only be usefully measured in simulations which explicitly use the vector potential $\mathbf{A}$. A similar invariant is the cross helicity

$$\int (\mathbf{B} \cdot \mathbf{v}) \mathrm{dV} \approx \sum_b m_b \frac{\mathbf{B}_b}{\rho_b} \cdot \mathbf{v}_b, \tag{4.16}$$

which measures the mutual linkage of magnetic field and vortex lines. The conservation of the cross helicity is a result of the magnetic field lines being frozen into the fluid. Measurement of the conservation of this quantity in a numerical simulation therefore provides an estimate of the degree of slippage of the magnetic field lines through the fluid. The volume integral of the magnetic flux

$$\int \mathbf{B} \mathrm{dV} \approx \sum_b m_b \frac{\mathbf{B}_b}{\rho_b} \tag{4.17}$$

is also conserved across the simulation volume, provided that the flux is normal to (or zero at) the boundary of the integration volume. However the conservation of flux in a volume sense is not particularly important physically (Janhunen, 2000). More important is that the surface integral of the flux

$$\int \mathbf{B} \cdot \mathrm{dS}, \tag{4.18}$$

should be conserved. Using the divergence theorem this corresponds to the conservation of the volume integral

$$\int (\nabla \cdot \mathbf{B}) \mathrm{dV} \approx \sum_b m_b \frac{(\nabla \cdot \mathbf{B})_b}{\rho_b}. \tag{4.19}$$

In the continuum case this conservation is exact since the divergence of the magnetic field is zero. However in a numerical scheme with non-zero magnetic divergence conservation of this quantity depends on the formulation of the induction equation with respect to the terms proportional to $\nabla \cdot \mathbf{B}$. Our induction equation (4.7) is formulated such that, even with non-zero $\nabla \cdot \mathbf{B}$ this quantity remains conserved (although this may differ slightly in the discrete equations), whereas (4.17) will only be approximately conserved.

There is also a conserved quantity which is the MHD analogue of the circulation (Bekenstein and Oron, 2000; Kuznetsov and Ruban, 2000), although the physical interpretation is somewhat obscure. It has been shown that SPH conserves an approximate version of the circulation in the hydrodynamic case (Monaghan and Price, 2001), related to the invariance of the equations to the relabelling of particles around a closed loop due to the frozen-in vorticity field (Salmon, 1988). A similar, though more restricted relabelling symmetry holds in the MHD case (in that the particles around the loop must also be on the same field line) and it may therefore be expected that SPMHD also maintains this invariance.

4.3 Smoothed Particle Magnetohydrodynamics

The discrete approximations to (4.1), (4.2), (4.7) and (4.11) are found by expressing the spatial derivatives as summations over the particles. As in the SPH case (§3.3, §3.4) we derive the SPMHD equations of motion and energy from a variational principle, in this case using the SPH forms of the continuity and induction equations as constraints. This ensures consistency between the discrete forms of the SPH equations (and hence also the continuum forms, removing the ambiguity with regard to terms proportional to the magnetic divergence) as well as adherence to physical principles.

4.3.1 Induction equation

The induction equation (4.7) in the absence of dissipation may be written in SPH form as

$$\frac{d\mathbf{B}_a}{dt} = \frac{1}{\rho_a}\sum_b m_b[\mathbf{B}_a(\mathbf{v}_{ab}\cdot\nabla_a W_{ab}) - \mathbf{v}_{ab}(\mathbf{B}_a\cdot\nabla_a W_{ab})]. \tag{4.20}$$

Alternatively we can use (4.9), written in the form

$$\frac{d}{dt}\left(\frac{\mathbf{B}}{\rho}\right) = \frac{1}{\rho^2}\left[(\mathbf{B}\cdot\nabla)\rho\mathbf{v} - \mathbf{v}(\mathbf{B}\cdot\nabla\rho)\right], \tag{4.21}$$

with SPH equivalent

$$\frac{d}{dt}\left(\frac{\mathbf{B}}{\rho}\right)_a = -\frac{1}{\rho_a^2}\sum_b m_b\mathbf{v}_{ab}(\mathbf{B}_a\cdot\nabla_a W_{ab}). \tag{4.22}$$

In the numerical tests presented in §4.6 we find little difference between the two forms (4.20) and (4.22) of the SPH induction equation. Many authors prefer to use (4.22) as the flux per unit mass $\mathbf{B}/\rho$ is a natural quantity to be carried by Lagrangian particles. There is some advantage in using (4.20) rather than (4.22) in one dimensional problems since using (4.20) ensures that the divergence of the magnetic field is exactly zero (since $B_x = \text{const}$). However the divergence errors associated with using (4.22)

in one dimension were found to be negligible for nearly all of the problems considered. Note that a 'conservative' form of the induction equation (as used in most grid-based MHD codes, although not a consistent formulation in the presence of magnetic monopoles) would correspond to a symmetric form of (4.22) (with the addition of a term $\mathbf{v}\nabla\cdot\mathbf{B}$), such that (4.17) is conserved but no longer implying the conservation of $\mathbf{B}/\rho$ along flow lines. An example of such a formalism is used in §5.3.2 in order to compare the divergence errors associated with various formulations of the MHD equations.

4.3.2 Equations of motion

Variational principles for MHD have been discussed by many authors (e.g. Newcomb 1962; Henyey 1982; Oppeneer 1984; Field 1986) and the Lagrangian is given by

$$L = \int \left(\frac{1}{2}\rho \mathrm{v}^2 - \rho u - \frac{1}{2\mu_0}B^2\right)\mathrm{dV}, \tag{4.23}$$

which is simply the kinetic minus the potential and magnetic energies. The SPH Lagrangian is therefore

$$L_{sph} = \sum_b m_b \left[\frac{1}{2}\mathrm{v}_b^2 - u_b(\rho_b, s_b) - \frac{1}{2\mu_0}\frac{B_b^2}{\rho_b}\right]. \tag{4.24}$$

where we have replaced the integral with a summation and the volume element $\rho\mathrm{dV}$ with the mass per SPH particle m. Ideally we would wish to express all the terms in the Lagrangian (4.24) in terms of the particle co-ordinates, which would automatically guarantee the conservation of momentum and energy since the equations of motion result from the Euler-Lagrange equations (e.g. Monaghan and Price 2001). The density can be written as a function of the particle coordinates using the usual SPH summation (3.42). The internal energy is regarded as a function of the density (via the first law of thermodynamics), which is in turn a function of the particle co-ordinates. However it is not intuitively obvious how the magnetic field $\mathbf{B}$ should be related to the particle co-ordinates, or even that it could be expressed in such a manner (in the SPH context this would imply an expression for $\mathbf{B}$ such that taking the time derivative gives (4.20) or (4.22), analogous to (3.42) for the density), though it could be done easily for a plasma with the electrons and ions described by separate sets of SPH particles. We may however proceed using the variational principle given for alternative formulations of SPH in §3.4, that is we require

$$\delta\int L\mathrm{dt} = \int \delta L\mathrm{dt} = 0, \tag{4.25}$$

where we consider variations with respect to a small change in the particle co-ordinates $\delta\mathbf{r}_a$. We therefore have

$$\delta L = m_a\mathbf{v}_a\cdot\delta\mathbf{v}_a - \sum_b m_b\left[\left.\frac{\partial u_b}{\partial\rho_b}\right|_s \delta\rho_b + \frac{1}{2\mu_0}\left(\frac{B_b}{\rho_b}\right)^2\delta\rho_b - \frac{1}{\mu_0}\mathbf{B}_b\cdot\delta\left(\frac{\mathbf{B}_b}{\rho_b}\right)\right]. \tag{4.26}$$

The Lagrangian variations in density and magnetic field are given by

$$\delta\rho_b = \sum_c m_c(\delta\mathbf{r}_b - \delta\mathbf{r}_c)\cdot\nabla_b W_{bc}, \tag{4.27}$$

$$\delta\left(\frac{\mathbf{B}_b}{\rho_b}\right) = -\sum_c m_c(\delta\mathbf{r}_b - \delta\mathbf{r}_c)\frac{\mathbf{B}_b}{\rho_b^2}\cdot\nabla_b W_{bc}, \tag{4.28}$$

where we have used (3.43) and (4.22) respectively (note that we also recover the following results if we use (4.20) instead of (4.22)). The perturbations given above correspond to SPH forms of the usual Lagrangian perturbations

$$\delta\rho = -\rho_0\nabla\cdot(\delta\mathbf{r}), \tag{4.29}$$

$$\delta\left(\frac{\mathbf{B}}{\rho}\right) = \frac{\mathbf{B}_0}{\rho_0}\cdot\nabla(\delta\mathbf{r}). \tag{4.30}$$

Using (4.27), (4.28) and the first law of thermodynamics (3.50) in (4.26) and rearranging, we find

$$\begin{aligned}\frac{\delta L}{\delta\mathbf{r}_a} &= -\sum_b m_b\left[\frac{P_b}{\rho_b^2}\sum_c m_c\nabla_b W_{bc}(\delta_{ba}-\delta_{ca})\right] - \sum_b m_b\left[\frac{1}{2\mu_0}\left(\frac{\mathbf{B}_b}{\rho_b}\right)^2\nabla_b W_{bc}(\delta_{ba}-\delta_{ca})\right] \\ &+ \sum_b m_b\left[\frac{1}{\mu_0}\frac{\mathbf{B}_b}{\rho_b^2}\sum_c m_c\mathbf{B}_b\cdot\nabla_b W_{bc}(\delta_{ba}-\delta_{ca})\right],\end{aligned} \tag{4.31}$$

where δ_{ab} refers to the Kronecker delta. Putting this back into (4.25), integrating the velocity term by parts and simplifying (using $\nabla_a W_{ab} = -\nabla_b W_{ba}$), we obtain

$$\begin{aligned}\int\Bigg\{-m_a\frac{d\mathbf{v}_a}{dt} &- \sum_b m_b\left(\frac{P_a}{\rho_a^2}+\frac{P_b}{\rho_b^2}\right)\nabla_a W_{ab} - \sum_b m_b\frac{1}{2\mu_0}\left(\frac{B_a^2}{\rho_a^2}+\frac{B_b^2}{\rho_b^2}\right)\nabla_a W_{ab} \\ &+ \sum_b m_b\frac{1}{\mu_0}\left[\frac{\mathbf{B}_a}{\rho_a^2}(\mathbf{B}_a\cdot\nabla_a W_{ab}) + \frac{\mathbf{B}_b}{\rho_b^2}(\mathbf{B}_b\cdot\nabla_a W_{ab})\right]\Bigg\}\delta\mathbf{r}_a dt = 0.\end{aligned} \tag{4.32}$$

The SPH equations of motion are therefore given by

$$\frac{d\mathrm{v}_a^i}{dt} = \sum_b m_b\left[\left(\frac{S^{ij}}{\rho^2}\right)_a + \left(\frac{S^{ij}}{\rho^2}\right)_b\right]\nabla_a^j W_{ab}, \tag{4.33}$$

where S^{ij} is the stress tensor (4.3). This form of the magnetic force term conserves linear momentum exactly (angular momentum is discussed below) but was shown by Phillips and Monaghan (1985) to be unstable under negative stresses, causing particles to clump together unphysically. The approach taken in this thesis is to remove the instability by adding a short range repulsive force which prevents particles from clumping, rather than sacrificing the conservation of momentum. The stability issues are discussed in detail in §4.4.

Note that using (4.33) for the magnetic force no longer guarantees that the magnetic force is perpendicular to $\mathbf{B}$, since the force (4.4) contains an additional term proportional to the divergence of $\mathbf{B}$. This non-zero force directed along the line joining the particles is essentially the physical cause of the clumping instability. It has been pointed out by Tóth (2000) in the context of grid based codes that if the momentum is conserved then the force will not be exactly perpendicular to $\mathbf{B}$ even if $\nabla\cdot\mathbf{B}$ is zero in a particular discretisation, since this does not imply that $\nabla\cdot\mathbf{B}$ is zero in every discretisation[1]. An example of this is in an SPH context is for purely one dimensional MHD, where even though $\nabla\cdot\mathbf{B} = 0$ (since

[1] although in a later paper Tóth (2002) has shown that both conditions *can* be met provided that the discretisation in which the divergence is zero is also the discretisation used in the force term.

B_x =const), the contribution from the divergence term in (4.33) is non-zero, resulting in an instability even in this simple case.

Finally, it should be noted that the conservative form of the momentum equation was derived using a non-conservative (in a volume sense, although conservative in a surface integral sense) induction equation, which agrees with the derivation of the MHD equations in the presence of magnetic monopoles given by Janhunen (2000) and Dellar (2001). This is discussed further in §5.2.1.

Angular momentum conservation

Whilst the conservation of linear momentum is maintained exactly for the formalism derived above, angular momentum conservation will not be exact since the force between the particles is not directed along the line joining them. Considering two dimensional motion in x and y, the change in angular momentum of the system is given by

$$\frac{d}{dt}\sum_a (\mathbf{r}_a \times \mathbf{v}_a)^z = \sum_a \sum_b m_a m_b \left(\left[\sigma_{ab}^{xx} - \sigma_{ab}^{yy} \right] y_{ab} x_{ab} + \sigma_{ab}^{xy} [y_{ab}^2 - x_{ab}^2] \right) F_{ab}, \tag{4.34}$$

where $y_{ab} = y_a - y_b$, $x_{ab} = x_a - x_b$ and $\sigma_{ab}^{ij} = S_a^{ij}/\rho_a^2 + S_b^{ij}/\rho_b^2$. We have replaced ∇W_{ab} by $\mathbf{r}_{ab} F_{ab}$. From (4.34) we see that the angular momentum will be conserved if the stress is isotropic and proportional to the identity tensor. However for more general stresses the angular momentum will change. It can be shown that upon translating the SPH expression (4.34) into continuum form (replacing the summations with integrals), angular momentum is conserved exactly.

The same problem arises in the case of elastic stresses where the problem is made worse by the fact that particles at the edge of the solid (which have no neighbours exterior to the solid to provide a full interpolation) have densities similar to the interior and consequently produce a significant error in the angular momentum. Bonet and Lok (1999) claim that normalising the kernel by a matrix factor similar to that described in §3.2.3 corrects for this error. A similar approach could be taken to the astrophysical problem, however we expect angular momentum conservation to be much better in this case without normalising the kernel because edges are associated with low density and correspondingly low angular momentum.

4.3.3 Energy equation

The Hamiltonian (3.59), using the Lagrangian (4.24) is given by

$$H = E = \sum_a m_a \left(\frac{1}{2} \mathrm{v}_a^2 + u_a + \frac{1}{2\mu_0} \frac{B_a^2}{\rho_a} \right). \tag{4.35}$$

Taking the (comoving) time derivative, we have

$$\frac{dE}{dt} = \sum_a m_a \left[\mathbf{v}_a \cdot \frac{d\mathbf{v}_a}{dt} + \frac{du_a}{d\rho_a}\frac{d\rho_a}{dt} + \frac{1}{2\mu_0}\frac{B_a^2}{\rho_a^2}\frac{d\rho_a}{dt} + \frac{\mathbf{B}_a}{\mu_0} \cdot \frac{d}{dt}\left(\frac{\mathbf{B}_a}{\rho_a} \right) \right], \tag{4.36}$$

where the first term is specified by use of the momentum equation (4.33), the second term using the first law of thermodynamics (3.50) and the continuity equation (3.43), the third term by the continuity

equation and the fourth term by the induction equation (4.22). Using these and simplifying we find

$$\frac{dE}{dt} = \sum_a m_a \sum_b m_b \left[\left(\frac{S^{ij}}{\rho^2} \right)_a \mathrm{v}_b^i + \left(\frac{S^{ij}}{\rho^2} \right)_b \mathrm{v}_a^i \right] \nabla_a^j W_{ab}, \tag{4.37}$$

such that the total energy per particle is evolved according to

$$\frac{de_a}{dt} = \sum_b m_b \left[\left(\frac{S^{ij}}{\rho^2} \right)_a \mathrm{v}_b^i + \left(\frac{S^{ij}}{\rho^2} \right)_b \mathrm{v}_a^i \right] \nabla_a^j W_{ab}, \tag{4.38}$$

where

$$e_a = \frac{1}{2}\mathrm{v}_a^2 + u_a + \frac{1}{2\mu_0}\frac{B_a^2}{\rho_a} \tag{4.39}$$

is the energy per unit mass. The internal energy equation follows from the use of the first law of thermodynamics and is therefore the same as in the hydrodynamic case (3.58) in the absence of dissipative terms. The equation for evolving the entropy (3.65) is also unchanged.

4.3.4 Alternative formulations

Consistent sets of SPMHD equations may also be derived using alternative forms of the continuity and induction equations as in §3.4. For example, using the continuity equation

$$\frac{d\rho_a}{dt} = \rho_a \sum_b m_b \frac{\mathbf{v}_{ab}}{\rho_b} \cdot \nabla_a W_{ab}, \tag{4.40}$$

and the induction equation

$$\frac{d}{dt}\left(\frac{\mathbf{B}}{\rho} \right)_a = -\frac{1}{\rho_a} \sum_b m_b \frac{\mathbf{v}_{ab}}{\rho_b} (\mathbf{B}_a \cdot \nabla_a W_{ab}). \tag{4.41}$$

results in the momentum equation

$$\frac{d\mathrm{v}_a^i}{dt} = \sum_b m_b \left[\frac{S_a^{ij} + S_b^{ij}}{\rho_a \rho_b} \right] \nabla_a^j W_{ab}. \tag{4.42}$$

This form of the SPMHD equations also conserves linear momentum exactly (and is hence also found to be unstable to the clumping instability). The variationally consistent internal energy equation is given by

$$\frac{du_a}{dt} = \frac{P_a}{\rho_a} \sum_b m_b \frac{\mathbf{v}_{ab}}{\rho_b} \cdot \nabla_a W_{ab}, \tag{4.43}$$

and the total energy equation by

$$\frac{de_a}{dt} = \sum_b m_b \left[\frac{S_a^{ij}\mathrm{v}_b^i + S_b^{ij}\mathrm{v}_a^i}{\rho_a \rho_b} \right] \nabla_a^j W_{ab}. \tag{4.44}$$

A general alternative formulation may also be derived, equivalent to that given in §3.4.

4.3.5 Vector formulations of the magnetic force

Earlier implementations of MHD in an SPH context used simple forms of the magnetic force terms based on the non-conservative force equation (4.5). The simplest form of the magnetic force term in (4.5) is derived by using the SPH summation interpolant for the magnetic field,

$$\mathbf{B}_a = \sum_b m_b \frac{\mathbf{B}_b}{\rho_b} W(\mathbf{r}_a - \mathbf{r}_b, h). \tag{4.45}$$

Taking the curl of this equation we have

$$\mathbf{J}_a = (\nabla \times \mathbf{B})_a = \sum_b m_b \nabla_a W_{ab} \times \frac{\mathbf{B_b}}{\rho_b}. \tag{4.46}$$

The magnetic force term is then given by

$$\begin{aligned} \left(\frac{\mathbf{J}\times\mathbf{B}}{\mu_0\rho}\right)_a &= (\nabla\times\mathbf{B})_a \times \frac{\mathbf{B}_a}{\mu_0\rho_a} \\ &= \sum_b m_b \left(\nabla_a W_{ab} \times \frac{\mathbf{B}_b}{\rho_b}\right) \times \frac{\mathbf{B}_a}{\mu_0\rho_a}. \end{aligned} \tag{4.47}$$

In SPH, however it is preferable to interpolate the curl using (c.f. §3.2.3)

$$\rho_a(\nabla\times\mathbf{B})_a = \sum_b m_b(\mathbf{B}_a - \mathbf{B}_b)\times\nabla_a W_{ab}, \tag{4.48}$$

and thus the magnetic force becomes

$$\frac{1}{\mu_0\rho_a^2}\sum_b m_b\,(\mathbf{B}_{ab}\times\nabla_a W_{ab})\times\mathbf{B}_a, \tag{4.49}$$

where $\mathbf{B}_{ab} = \mathbf{B}_a - \mathbf{B}_b$. This 'vector' form of the magnetic force term has been used by many authors (e.g. Meglicki et al., 1995; Byleveld and Pongracic, 1996; Cerqueira and de Gouveia Dal Pino, 2001; Hosking and Whitworth, 2004). Using this formulation the magnetic force is always perpendicular to the magnetic field but exact conservation of momentum is not guaranteed. Equation (4.49) may also be expressed as:

$$\frac{1}{\mu_0\rho_a^2}\sum_b m_b\left[(\mathbf{B}_{ab}\cdot\mathbf{B}_a)\nabla_a W_{ab} - (\mathbf{B}_a\cdot\nabla_a W_{ab})\mathbf{B}_{ab}\right]. \tag{4.50}$$

Whilst this results in a stable numerical scheme, the lack of momentum conservation in this formalism means that it gives extremely poor results on problems involving shocks. We also note that this is the discretisation of a pure $\mathbf{J}\times\mathbf{B}$ force which, as discussed in §4.2.1 does not represent a consistent formulation of the magnetic force in the presence of monopoles.

4.3.6 Variable smoothing length terms

Since we cannot explicitly write the Lagrangian (4.24) as a function of the particle co-ordinates, we cannot explicitly derive the SPMHD equations incorporating a variable smoothing length. We may,

however deduce the form of the terms which should be included by consistency arguments. We start with the SPH induction equation in the form

$$\frac{d}{dt}\left(\frac{\mathbf{B}}{\rho}\right)_a = -\frac{1}{\rho_a^2}\sum_b m_b \mathbf{v}_{ab}(\mathbf{B}_a \cdot \nabla_a W_{ab}). \tag{4.51}$$

Expanding the left hand side, we have

$$\frac{d\mathbf{B}_a}{dt} = -\frac{1}{\rho_a}\sum_b m_b \mathbf{v}_{ab}(\mathbf{B}_a \cdot \nabla_a W_{ab}) + \frac{\mathbf{B}_a}{\rho_a}\frac{d\rho_a}{dt}. \tag{4.52}$$

If the smoothing length is a given function of the density, then the SPH continuity equation is given by (3.70) and (4.52) becomes

$$\frac{d\mathbf{B}_a}{dt} = -\frac{1}{\rho_a}\sum_b m_b \left\{\mathbf{v}_{ab}(\mathbf{B}_a \cdot \nabla_a W_{ab}) - \frac{1}{\Omega_a}\mathbf{B}_a[\mathbf{v}_{ab} \cdot \nabla_a W_{ab}(h_a)]\right\}. \tag{4.53}$$

where Ω is defined in §3.3.4. However in one dimension these terms must cancel to give $B_x = \text{const}$, and thus we deduce that the correct form of the induction equation is therefore

$$\frac{d\mathbf{B}_a}{dt} = -\frac{1}{\Omega_a\rho_a}\sum_b m_b \left\{\mathbf{v}_{ab}\left[\mathbf{B}_a \cdot \nabla_a W_{ab}(h_a)\right] - \mathbf{B}_a\left[\mathbf{v}_{ab} \cdot \nabla_a W_{ab}(h_a)\right]\right\}, \tag{4.54}$$

or in the form (4.51) we would have

$$\frac{d}{dt}\left(\frac{\mathbf{B}}{\rho}\right)_a = -\frac{1}{\Omega_a\rho_a^2}\sum_b m_b \mathbf{v}_{ab}[\mathbf{B}_a \cdot \nabla_a W_{ab}(h_a)]. \tag{4.55}$$

Using (4.54) or (4.55) and (3.70) as constraints we may then derive the equations of motion using the variational principle described in §3.3.2 to give

$$\frac{d\mathrm{v}_a^i}{dt} = \sum_b m_b \left[\left(\frac{S^{ij}}{\Omega\rho^2}\right)_a \nabla_a^j W_{ab}(h_a) + \left(\frac{S^{ij}}{\Omega\rho^2}\right)_b \nabla_a^j W_{ab}(h_b)\right]. \tag{4.56}$$

The total energy equation is given by

$$\frac{de_a}{dt} = \sum_b m_b \left[\left(\frac{S^{ij}}{\Omega\rho^2}\right)_a \mathrm{v}_b^i \nabla_a^j W_{ab}(h_a) + \left(\frac{S^{ij}}{\Omega\rho^2}\right)_b \mathrm{v}_a^i \nabla_a^j W_{ab}(h_b)\right], \tag{4.57}$$

whilst the internal energy equation is found using the first law of thermodynamics and (3.70), that is

$$\frac{du_a}{dt} = \frac{P_a}{\Omega_a\rho_a^2}\sum_b m_b \mathbf{v}_{ab} \cdot \nabla_a W_{ab}(h_a) \tag{4.58}$$

We show in §4.6.4 that including the correction terms for a variable smoothing length in this manner significantly improves the numerical wave speed in the propagation of MHD waves and enables the shock tube problems considered in §4.6.3 to be computed with no smoothing of the initial conditions.

4.4 Stability

A full stability analysis of the SPMHD equations for negative stress has been presented by Morris (1996). The simplest MHD case is for a purely one dimensional problem, where $\mathbf{B} = [B_x, 0, 0]$. In this case the dispersion relation is easily obtained from the hydrodynamic version (3.41) by simply replacing the pressure P by $P - \frac{1}{2}B_x^2$, giving

$$\begin{aligned}\omega_a^2 &= \frac{2m(P_0 - \frac{1}{2}B_x^2)}{\rho_0^2}\sum_b [1-\cos k(x_a - x_b)]\frac{\partial^2 W}{\partial x^2}(x_a - x_b, h) \\ &\quad + \frac{m^2}{\rho_0^2}\left(c_s^2 - \frac{2(P_0 - \frac{1}{2}B_x^2)}{\rho_0}\right)\left[\sum_b \sin k(x_a - x_b)\frac{\partial W}{\partial x}(x_a - x_b, h)\right]^2, \end{aligned} \tag{4.59}$$

where as previously $c_s^2 = \partial P/\partial\rho$. Following Morris (1996), we define the negative stress parameter

$$\mathscr{R} = 1 - \frac{\frac{1}{2}B_x^2}{P_0} \tag{4.60}$$

such that $\mathscr{R} = 1$ corresponds to the hydrodynamic case and $\mathscr{R} < 0$ corresponds to negative stress. The dispersion relation for an isothermal gas ($c_s^2 = P/\rho$) is then given by

$$\begin{aligned}\omega_a^2 &= \frac{2mc_s^2}{\rho_0}\mathscr{R}\sum_b [1-\cos k(x_a - x_b)]\frac{\partial^2 W}{\partial x^2}(x_a - x_b, h) \\ &\quad + \left(\frac{mc_s}{\rho_0}\right)^2 (1 - 2\mathscr{R})\left[\sum_b \sin k(x_a - x_b)\frac{\partial W}{\partial x}(x_a - x_b, h)\right]^2. \end{aligned} \tag{4.61}$$

Figure 4.1 shows contours of the (normalised) square of the numerical sound speed $C_{num}^2 = \omega^2/k^2$ from this dispersion relation evaluated for the cubic spline kernel at a fixed value of smoothing length ($h = 1.2\Delta p$). The contours are shown as a function of wavenumber (in units of the average particle spacing) and the negative stress parameter $\mathscr{R}$[2]. As in §3.2.7, sums in (4.61) are calculated numerically (rather than making any further approximations) assuming an isothermal sound speed and particle spacing of unity (where both wavelength and smoothing length are calculated in units of the particle spacing). From Figure 4.1 we observe that the kernel is unstable to negative stress ($\mathscr{R} < 0$) at short wavelengths, with the instability first occurring at a wavenumber $k = \pi$ (corresponding to a wavelength of twice the particle spacing Δp). Note that these results are very similar for other smoothing length values and for all of the kernels considered in §3.2.

In a numerical simulation, this instability manifests as particles clumping together, beginning at short wavelengths but quickly destroying the simulation (Figure 4.2). Since the one dimensional MHD case involves only a constant magnetic pressure subtracted from the gas pressure, the source of the instability can be traced to non-cancellation of the first error term (which is non-zero even for constant functions) in the SPH approximation when a momentum-conserving form of the gradient evaluation is used (refer to the discussion in §3.2.3). Indeed using a differencing form for the gradient term such as (3.16) results in a stable formalism, but in this case the exact conservation of momentum is lost (although a compromise approach is described below, §4.4.2).

[2] this figure corresponds to Figure 2.1 in Morris (1996)

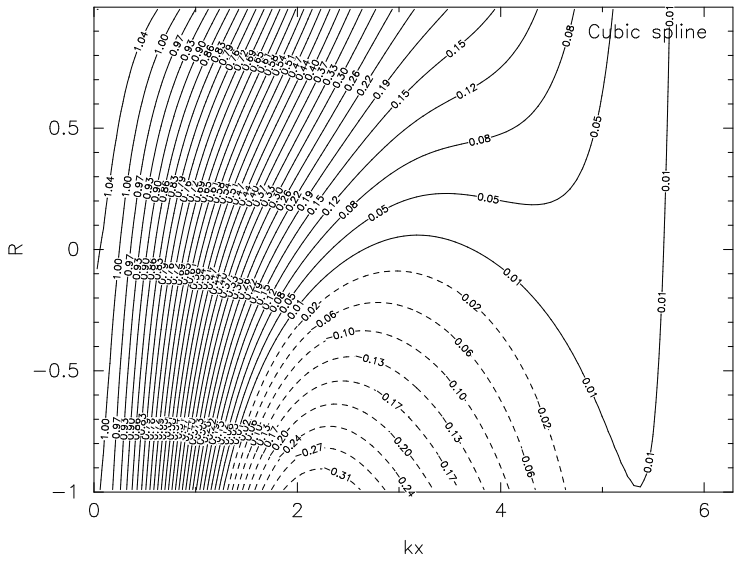

Figure 4.1: One dimensional stability properties of the cubic spline kernel with respect to the negative stress parameter $\mathscr{R} = (1 - \frac{1}{2}B_x^2/P)$ (y-axis). The x-axis corresponds to wavenumber in units of $1/\Delta x$ (such that $kx \rightarrow 0$ represents the limit of an infinite number of particles per wavelength). Contours show the (normalised) square of the numerical wave speed from the dispersion relation (4.59). The kernel is unstable to negative stress ($\mathscr{R} < 0$) at short wavelengths.

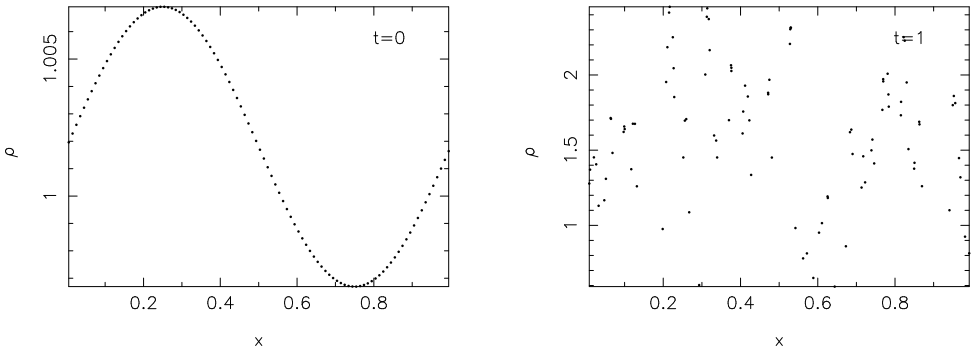

Figure 4.2: Results of a one dimensional isothermal sound wave simulation with a constant magnetic field in the $x-$direction such that $\mathscr{R} = -1$. The initial conditions are shown in the left panel, using 100 particles with an initial amplitude of 0.5%. The wave quickly becomes unstable due to the negative stress and the results are shown in the right panel after one period.

Since conservation of momentum is important for the accurate simulation of shocks, several remedies for this instability, associated with the tensor (ie. momentum-conserving) form of the magnetic force term have been suggested. In their initial investigation Phillips and Monaghan (1985) used a simple 'regularization' technique - that is they swept over the particles to find the maximum value of the magnetic component of the stress tensor (4.3) and then subtracted this from the stress tensor in (4.33). Recently, however, it has been shown that a similar instability occurs when SPH is used in solid mechanics simulations where again there is an anisotropic stress. The instability occurs when the particles are in tension (ie. the stress is negative) and again leads to a clumping effect, analogous to the MHD instability. Several remedies have been proposed in the engineering literature (e.g. Dyka et al. 1997; Bonet and Kulasegaram 2000, 2001) but they all either involve a significant increase in computation or cannot be applied where the particle configuration changes significantly (for a more detailed discussion see Monaghan, 2000).

A remedy for the tensile instability which does not require additional computational expense and can be easily applied to astrophysical problems was proposed by Monaghan (2000) and we investigate this technique below.

4.4.1 Anti-clumping term

The idea proposed by Monaghan (2000) is add a term which prevents particles clumping under negative stress. Since the instability occurs at short wavelengths, this term should modify the stress at small particle spacings so as to provide a repulsive force which prevents the particles clumping together under tension forces (negative stress). Determining whether or not the particles are in tension is determined by rotating into co-ordinates which lie along the principal stress axis (ie. where the stress tensor is diagonal). The magnetic stress tensor is diagonal when the magnetic field lies along one of the co-ordinate axes (which in this case we assume to be the $x-$axis). The magnetic field is then $\mathbf{B}' = (B,0,0)$ and the stress tensor has non zero components $M'_{xx} = B^2/(2\mu_0)$, $M'_{yy} = -B^2/(2\mu_0)$, and $M'_{zz} = -B^2/(2\mu_0)$. The positive component in the $x-$component indicates tension, whilst the negative components in the $y-$ and $z-$ directions indicate compression. To remove the tension term at close range a term is added to M'_{xx} so that it is negative when the particles approach. The term added is RB^2, where

$$R = -\frac{\varepsilon}{2\mu_0}\left(\frac{W_{ab}}{W_1}\right)^n, \tag{4.62}$$

where W is the SPH kernel and W_1 is the kernel evaluated at the average particle spacing (a constant). Rotating back to the original co-ordinate system, this is equivalent to defining a new magnetic stress

$$M'_{ij} = M_{ij} + RB_iB_j. \tag{4.63}$$

The momentum equation (4.33) becomes

$$\frac{dv^i_a}{dt} = \sum_b m_b \left\{ \left(\frac{S_{ij}}{\rho^2}\right)_a + \left(\frac{S_{ij}}{\rho^2}\right)_b + R\left[\left(\frac{B_iB_j}{\rho^2}\right)_a + \left(\frac{B_iB_j}{\rho^2}\right)_b\right]\right\}\frac{\partial W_{ab}}{\partial x_{j,a}}. \tag{4.64}$$

In the preceding discussion, we have interpreted the artificial stress term as a modification of the anisotropic component of the magnetic stress tensor. An alternative interpretation (and one which we prefer) is to regard it as a modification to the kernel gradient in the anisotropic force at small particle spacings. The momentum equation may then be expressed as

$$\begin{aligned}\frac{dv^i_a}{dt} &= -\sum_b m_b\left[\left(\frac{P}{\rho^2}+\frac{B^2}{2\mu_0\rho^2}\right)_a + \left(\frac{P}{\rho^2}+\frac{B^2}{2\mu_0\rho^2}\right)_b\right]\frac{\partial W_{ab}}{\partial x_{j,a}} \\ &\quad + \sum_b \frac{m_b}{\mu_0}\left[\left(\frac{B_iB_j}{\rho^2}\right)_a + \left(\frac{B_iB_j}{\rho^2}\right)_b\right]\frac{\partial Y_{ab}}{\partial x_{j,a}},\end{aligned} \tag{4.65}$$

where $\partial Y_{ab}/\partial x$ is the modified kernel gradient, given by

$$\frac{\partial Y_{ab}}{\partial x} = \left[1 - \frac{\varepsilon}{2}\left(\frac{W_{ab}}{W_1}\right)^n\right]\frac{\partial W_{ab}}{\partial x} \tag{4.66}$$

The effect of the anticlumping term on the kernel gradient is shown in Figure 4.3 for various values of ε

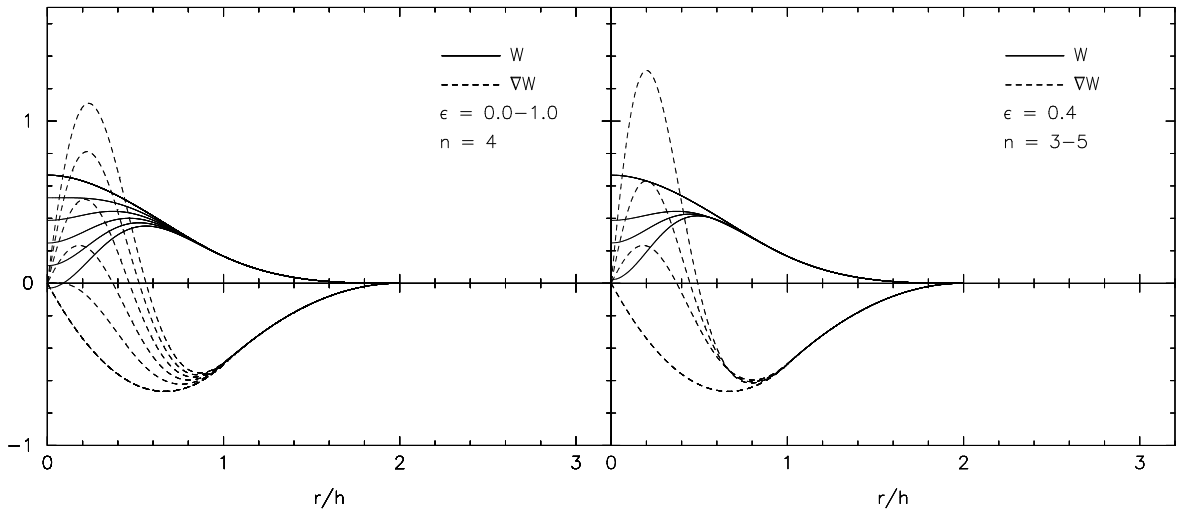

Figure 4.3: Effect of the anticlumping term on the kernel gradient in the anisotropic magnetic force. The cubic spline kernel (solid line) and its first derivative (dashed) are shown as modified by the anticlumping term. The left panel shows the effect of varying ε (shown in steps of 0.2 from $\varepsilon = 0.0$ to $\varepsilon = 1.0$) whilst the right panel shows the effect of varying the index n (shown for $n = 3, 4$ and 5, with the unmodified kernel shown for comparison). The constant kernel in the denominator, W_1, is evaluated at $r/h = 1/1.5$. The modification of the kernel gradient shown in this figure is used when computing the anisotropic magnetic force to prevent the particles from clumping unphysically. The modified kernel itself is not used in the calculations and is plotted for comparison only.

and n. This modified gradient is *only* used in the anisotropic magnetic force and does not therefore affect the calculation of hydrodynamic and isotropic magnetic forces.

The function R is designed to increase as the particle separation decreases. The kernel gradients in Figure (4.3) are shown for a smoothing length of $h = 1.5\Delta p$ and therefore in (4.62) the kernel in the denominator is computed using $\Delta p/h = 1/1.5$. In the one dimensional numerical tests described in §4.6 simulations using this value of smoothing length, use of the anticlumping term was found to give good results with few side effects. In two and three dimensions, however, more typical values for h are in the range $1.1 - 1.2\Delta p$, in order to reduce the number of neighbours required in the summations (and thus the computational expense). Re-running the one dimensional shock simulations with these values for h, it was found that the artificial stress term produced pronounced errors in the shock profiles (this is discussed further in §4.6.3 and demonstrated in Figure 4.13). For this reason we find it is better to interpret $W(\Delta p)$ as the kernel evaluated at a particular fixed radius, rather than at the average particle spacing. We therefore use $r/h = 1/1.5$ in $W(\Delta p)$ independent of the choice of smoothing length. That this provides a significant improvement in the results is also demonstrated in Figure (4.6) from the results of a stability analysis of the SPMHD equations incorporating the anticlumping term. The stability analysis is given below.

Stability analysis with anticlumping term

A one-dimensional stability analysis of SPH including an artificial stress term is given by Monaghan (2000). With the artificial stress interpreted as a modification to the kernel gradient on the anisotropic force, the one dimensional dispersion relation for MHD is easily obtained from the hydrodynamic version

(3.41) by assuming a pressure of the form $P = P_{iso} + P_{aniso}$, where in this case we have $P_{iso} = P + \frac{1}{2}B_x^2$ and $P_{aniso} = -B_x^2$. The resulting dispersion relation is given by

$$\begin{aligned}\omega_a^2 &= \frac{2mP_{iso}}{\rho_0^2}\sum_b [1-\cos k(x_a-x_b)]\frac{\partial^2 W_{ab}}{\partial x^2} \\ &+\frac{m^2}{\rho_0^2}\left(c_s^2 - \frac{2P_{iso}}{\rho_0}\right)\left[\sum_b \sin k(x_a-x_b)\frac{\partial W_{ab}}{\partial x}\right]^2 \\ &+\frac{2mP_{aniso}}{\rho_0^2}\sum_b [1-\cos k(x_a-x_b)]\frac{\partial^2 Y_{ab}}{\partial x^2} \\ &-\frac{m^2}{\rho_0^2}\left(\frac{2P_{aniso}}{\rho_0}\right)\left[\sum_b \sin k(x_a-x_b)\frac{\partial W_{ab}}{\partial x}\right]\left[\sum_b \sin k(x_a-x_b)\frac{\partial Y_{ab}}{\partial x}\right], \end{aligned} \tag{4.67}$$

where the modified kernel Y and its derivatives are given by

$$Y_{ab} = \left[1-\frac{\varepsilon}{2(n+1)}\left(\frac{W_{ab}}{W_1}\right)^n\right]W_{ab}, \tag{4.68}$$

$$\frac{\partial Y_{ab}}{\partial x} = \left[1-\frac{\varepsilon}{2}\left(\frac{W_{ab}}{W_1}\right)^n\right]\frac{\partial W_{ab}}{\partial x}, \tag{4.69}$$

$$\frac{\partial^2 Y_{ab}}{\partial x^2} = \frac{\partial^2 W_{ab}}{\partial x^2} - \frac{\varepsilon}{(n+1)W_1^n}\frac{\partial^2 W_{ab}^{n+1}}{\partial x^2}. \tag{4.70}$$

Figure 4.4 shows contours of the square of the numerical sound speed $C_{num}^2 = \omega^2/k^2$ from this dispersion relation as a function of wavenumber and the negative stress parameter $\mathscr{R}$ (where in this case we have $P_{iso}/\rho_0 = c_s^2(2-\mathscr{R})$ and $P_{aniso}/\rho_0 = 2c_s^2(\mathscr{R}-1)$) for an isothermal equation of state, using $n = 4$ and six different values of ε. The top left panel ($\varepsilon = 0.0$) corresponds to Figure 4.1, except that the $y-$axis extends to $\mathscr{R} = -10$ in this case. Results are shown for a fixed smoothing length of $h = 1.2\Delta p$, however as discussed above the constant kernel in the denominator, W_1, is evaluated at $r/h = 1/1.5$. This means that the kernel used on the anisotropic term corresponds to those shown in Figure (4.3). We observe that for this value of n the formalism is stabilised for $\varepsilon \gtrsim 0.3$ and this is confirmed by numerical simulations (Figure 4.5). However, whereas in the $\varepsilon = 0.0$ case the contours near $k_x = 0$ are close to unity, in Figure (4.1) the numerical wave speed appears to increase substantially with increasing negative stress ($\mathscr{R} \to -\infty$). Thus, although the formalism is stabilised at short wavelengths, the wave speed at long wavelengths is also affected slightly.

This effect is illustrated further in Figure (4.6), where we plot the numerical sound speed versus $\mathscr{R}$ at $k_x \approx 0$ taken from Figure (4.1) (solid line) for $h = 1.2\Delta p$. The results using W_1 evaluated at the average particle spacing (ie at $r/h = 1/1.2$ in this case) as in the original formulation of Monaghan (2000) are also shown (dashed line). In both cases the wave speed is increases substantially as $\mathscr{R}$ becomes more negative, although the former case is a significant improvement over the latter. To confirm that the analytic stability analysis is an accurate representation of numerical results, we also plot the results of 12 simulations of small amplitude (0.5%) isothermal sound waves (as described in §3.7.2) with a constant magnetic field in the $x-$direction corresponding to various values of $\mathscr{R}$. The numerical results (solid points) show excellent agreement with the analytic dispersion relation.

To understand the increase in wave speed with decreasing $\mathscr{R}$ caused by the anticlumping term, it is

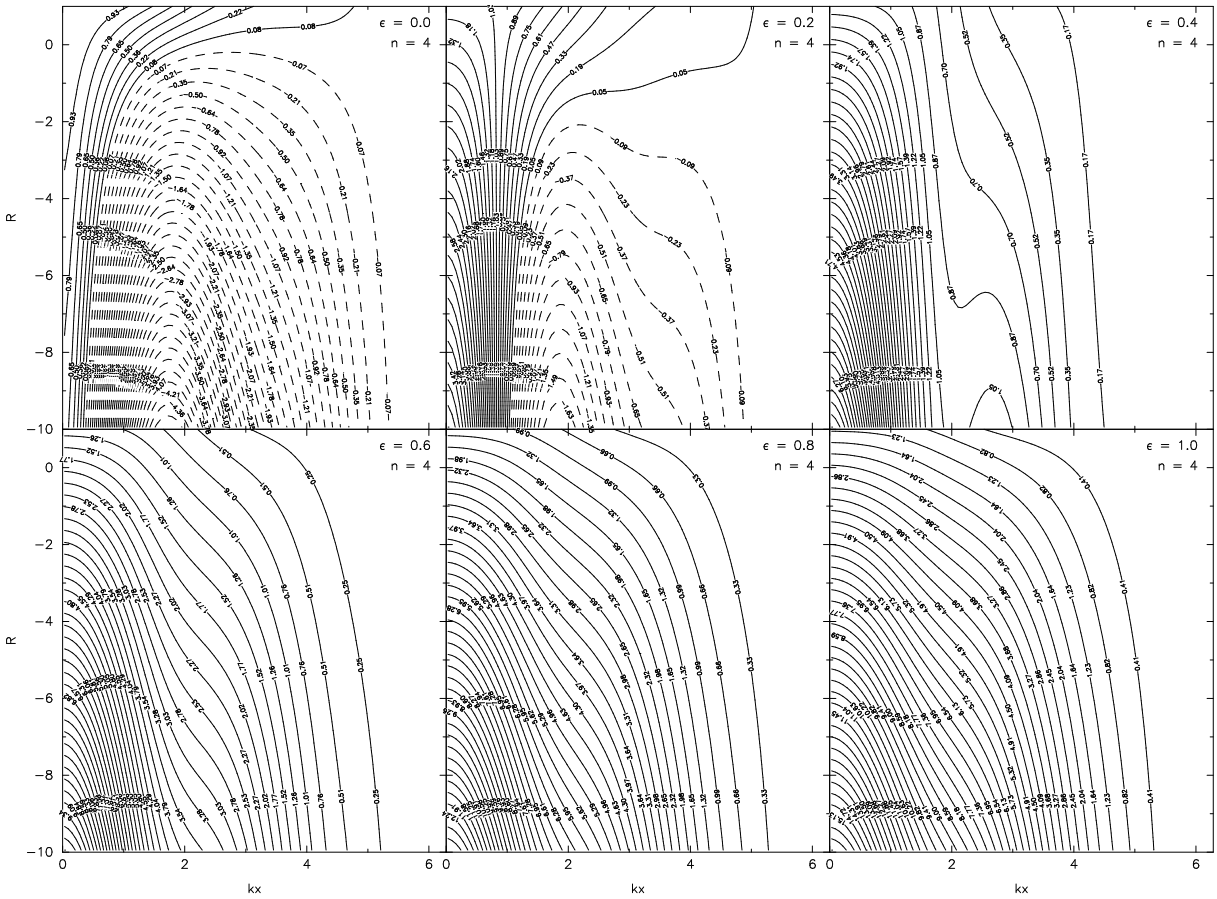

Figure 4.4: Effect of the anticlumping term on the one dimensional stability properties of the cubic spline kernel for various values of ε and n (as indicated in legend). Contours show the square of the numerical sound speed from the dispersion relation (4.67) as a function of the negative stress parameter $\mathscr{R} = (1 - \frac{1}{2}B_x^2/P)$ ($y-$axis) and the wavenumber in units of the particle spacing. Results are for a fixed smoothing length of $h = 1.2\Delta p$, with W_1 evaluated at $r/h = 1.5$.

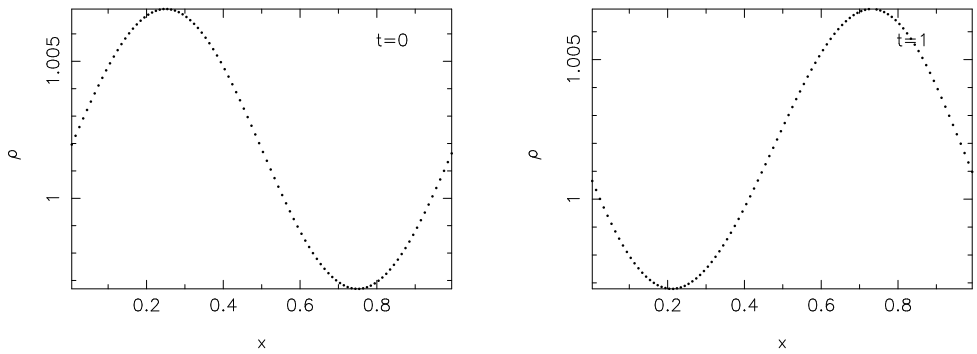

Figure 4.5: A repeat of the isothermal sound wave simulation shown in Figure 4.2 (with $\mathscr{R} = -1$) using the anticlumping term with parameters $\varepsilon = 0.4, n = 4$. The initial conditions are shown in the left panel, using 100 particles with an initial amplitude of 0.5%. The results after one period are shown in the right panel and are clearly stabilised by the anticlumping term, although the wave exhibits a significant phase error.

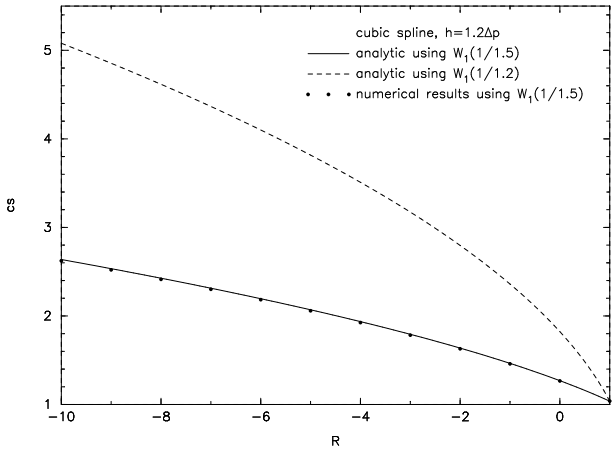

Figure 4.6: Numerical sound speed vs negative stress parameter R for the cubic spline kernel with a fixed smoothing length of $h = 1.2\Delta p$ and anticlumping parameters $\varepsilon = 0.4$, $n = 4$. The solid and dashed lines show the results at $k_x \approx 0$ from the dispersion relation (4.67), with the kernel in the denominator of the anticlumping term evaluated at the average particle spacing (dashed line) and at the fixed radius 1/1.5 (solid line), as discussed in the text. In the latter case the analytic results may be compared with the solid points from numerical simulations. The close agreement between the two demonstrates that the analytic stability analysis is a faithful representation of the numerical results.

instructive at to consider (4.67) in the limit of $k \to 0$ (ie. at long wavelengths). In this case we have $\sin k(x_a - x_b) \approx k(x_a - x_b)$ and $\cos k(x_a - x_b) \approx 1 - \frac{1}{2}k^2(x_a - x_b)^2$, giving

$$\begin{aligned}\omega_a^2/k_x^2 &= \frac{mP_{iso}}{\rho_0^2}\sum_b (x_a - x_b)^2 \frac{\partial^2 W_{ab}}{\partial x^2} + \frac{m^2}{\rho_0^2}\left(c_s^2 - \frac{2P_{iso}}{\rho_0}\right)\left[\sum_b (x_a - x_b)\frac{\partial W_{ab}}{\partial x}\right]^2 \\ &\quad + \frac{mP_{aniso}}{\rho_0^2}\sum_b (x_a - x_b)^2 \frac{\partial^2 Y_{ab}}{\partial x^2} - \frac{m^2}{\rho_0^2}\left(\frac{2P_{aniso}}{\rho_0}\right)\left[\sum_b (x_a - x_b)\frac{\partial W_{ab}}{\partial x}\right]\left[\sum_b (x_a - x_b)\frac{\partial Y_{ab}}{\partial x}\right] \quad (4.71)\end{aligned}$$

The accuracy of the numerical sound speed in this limit (which is the limit of an infinite number of particles, but not an infinite number of neighbours) is governed by the extent to which, for each kernel, the following normalisation conditions hold on the gradients:

$$\sum_b \frac{m_b}{\rho_b}(x_a - x_b)\frac{\partial W_{ab}}{\partial x} \approx 1, \qquad \text{and} \qquad \frac{1}{2}\sum_b \frac{m_b}{\rho_b}(x_a - x_b)^2 \frac{\partial^2 W_{ab}}{\partial x^2} \approx 1. \quad (4.72)$$

In the limit of an infinite number of neighbours (ie. $h \to \infty$) the summations can be written as integrals and the normalisations take the form

$$\int (x - x')\frac{\partial W}{\partial x}\mathrm{dx}' = 1 \qquad \text{and} \qquad \frac{1}{2}\int (x - x')^2 \frac{\partial^2 W}{\partial x^2}\mathrm{dx}' = 1. \quad (4.73)$$

It may be easily verified by the reader that setting the corresponding expressions to unity in (4.71) (for both kernels) gives the exact dispersion relation for sound waves (ie. $\omega^2 = k_x^2 c_s^2$). A straightforward integration for the cubic spline kernel demonstrates that both of these integrals hold on account of the normalisation condition (3.4) and the fact that the kernel is even. Considering the modified kernel gradient used in the anticlumping term (4.69)-(4.70), the normalisations can no longer hold because the kernel gradient is no longer normalised. The approach taken to this problem in Monaghan (2000) is to

simply choose the index n so as to minimise the term multiplying these integrals, giving n in the range $3 \leq n \leq 7$. Naively, one might expect that a renormalising the modified kernel gradient so as to maintain the integrals (4.73) would increase the accuracy of the simulation results. However in practise we find that this is not the case, since the summations (4.72) only sample the integrals at a few points. As such the renormalisation can have detrimental effects because it changes the kernel gradient at large r/h to compensate for the changing shape at small r/h, affecting more than the nearest neighbours.

In the hydrodynamic case it was found that allowing the smoothing length to vary could significantly improve the numerical wave speeds (§3.7.2). In the case of a variable smoothing length, three options are available for the modified kernel gradient: to use the average of the smoothing lengths, the average of the kernel gradients or thirdly to use the consistent formulation including the variable smoothing length terms (§4.3.6), in this case evaluated for the modified kernel gradient. Since the variable smoothing length terms effectively normalise the kernel gradient, the latter would seem to be a particularly good approach, particularly in the light of the discussion in the previous section. However, the one (somewhat large) caveat to the anticlumping approach is that, using variable smoothing lengths, we do not find that the anticlumping term guarantees numerical stability for all values of negative stress. For example, using the average smoothing length in (all of) the kernel gradients, the one dimensional sound waves become unstable at $\mathscr{R} \lesssim -9$. Using the average of the gradients the problem is worse and the waves become unstable at $\mathscr{R} \lesssim -3$. With the variable smoothing length terms calculated independently for both kernels, instability is observed at $\mathscr{R} \lesssim -2$. It would seem therefore, that although sufficient to provide numerical stability for all of the test problems considered here, the anticlumping approach as it stands does not provide a comprehensive solution. For this reason we compare this approach to two other methods described in §4.4.2 and §4.4.4 and in fact the multidimensional tests described in Chapter 5 suggest that these methods both give better results than use of the anticlumping term.

Implementation

The anticlumping term is implemented in this thesis by calculating the modified kernel gradient in a similar manner to the usual kernel. This is also the most cost-effective implementation since the modified kernel can be pre-computed and tabulated as for the usual kernel.

Where the total energy equation (4.38) is used, the contribution to the total energy from the anti-clumping term must be added for consistency. This can be found using (4.36) and is given by

$$\left(\frac{de_a}{dt}\right)_{src} = \sum_b m_b \mathrm{v}_a^i R \left[\left(\frac{B_i B_j}{\rho^2}\right)_a + \left(\frac{B_i B_j}{\rho^2}\right)_b\right] \frac{\partial W_{ab}}{\partial x_{j,a}}. \tag{4.74}$$

Alternatively, interpreting the anticlumping term as a modified kernel gradient, the contribution to the total energy from the anisotropic term in (4.38) is replaced by

$$\left(\frac{de_a}{dt}\right)_{aniso} = \sum_b m_b \left(\frac{B_a^i B_a^j}{\rho_a^2} \mathrm{v}_b^i \nabla^j W_{ab} + \frac{B_b^i B_b^j}{\rho_b^2} \mathrm{v}_a^i \nabla^j Y_{ab}\right) + \sum_b m_b \frac{B_a^i B_a^j}{\rho_a^2} \mathrm{v}_a^i \left(\nabla^j Y_{ab} - \nabla^j W_{ab}\right). \tag{4.75}$$

In principle it is possible to conserve total energy exactly by also using the modified kernel gradient in the $\mathbf{B}/\rho$ version of the induction equation (giving $W_{ab} = Y_{ab}$ in the above). However this introduces

an unnecessary alteration to the magnetic field evolution and consequently produces undesirable side effects. The degree to which energy conservation is violated when the total energy equation is evolved may therefore be used as an indication of the relative error introduced by the anticlumping term. In general this is found to be quite small for the problems considered in this thesis.

4.4.2 Morris approach

An alternative approach suggested by Morris (1996) is to retain the conservation of momentum on the isotropic terms in (4.33) but to treat the anisotropic terms using a differencing formalism which is exact in the case of a constant functions (see §3.2.3). The force term is then given by

$$-\sum_b m_b \left(\frac{P_a + \frac{1}{2}B_a^2/\mu_0}{\rho_a^2} + \frac{P_b + \frac{1}{2}B_b^2/\mu_0}{\rho_b^2} \right) \frac{\partial W_{ab}}{\partial x^i} + \frac{1}{\mu_0} \sum_b m_b \frac{(B_i B_j)_b - (B_i B_j)_a}{\rho_a \rho_b} \frac{\partial W_{ab}}{\partial x_j}. \tag{4.76}$$

This formalism does not therefore guarantee exact momentum conservation (since the anisotropic term does not give equal and opposite forces between particle pairs) but can be expected to give good results on shocks for which the anisotropic term is less important. It is also a better approach than the vector-based formalisms (§4.3.5) since (4.76) is still a discretisation of a tensor force and therefore conserves momentum in the continuum limit for non-zero $\nabla \cdot \mathbf{B}$. This also means that (4.76) retains the consistent formulation of the MHD equations in the presence of monopoles, although the discrete equations are no longer self-consistent with each other. Note that when using the variable smoothing length terms, we use the average of the normalised kernel gradient in (4.76), as in the dissipative terms. The dispersion relation for this formalism in the case of one dimensional MHD takes a particularly simple form since the terms resulting from the anisotropic force are zero in the case of $B_x =$const, giving

$$\begin{aligned} \omega_a^2 &= \frac{2mP_{iso}}{\rho_0^2} \sum_b [1 - \cos k(x_a - x_b)] \frac{\partial^2 W_{ab}}{\partial x^2} \\ &\quad + \frac{m^2}{\rho_0^2} \left(c_s^2 - \frac{2P_{iso}}{\rho_0} \right) \left[\sum_b \sin k(x_a - x_b) \frac{\partial W_{ab}}{\partial x} \right]^2. \end{aligned} \tag{4.77}$$

Contours of the square of the numerical sound speed $C_{num}^2 = \omega^2/k_x^2$ from this dispersion relation are shown in Figure (4.7). The formalism is seen to be stable for all wavelengths and this is confirmed by numerical simulations. Also the numerical wave speed does not show the increase with increasing negative stress observed for the anticlumping term, although the numerical wave speed is somewhat overestimated at short wavelengths $k_x \sim \pi/2\Delta x$. The more accurate numerical wave speeds result from the use of the differencing formalism since in this case the zeroth order error terms for small perturbations are zero exactly (§3.2.3). However, the main test of this formalism is the degree to which the lack of momentum conservation affects the shock capturing ability of the scheme. This is examined and compared with the anticlumping approach in the shock tube tests described in §4.6 where in fact the differences are found to be very minor. This simple approach is therefore a very viable solution which guarantees numerical stability in all circumstances and does not suffer from the numerical wave speed errors introduced by the anticlumping term.

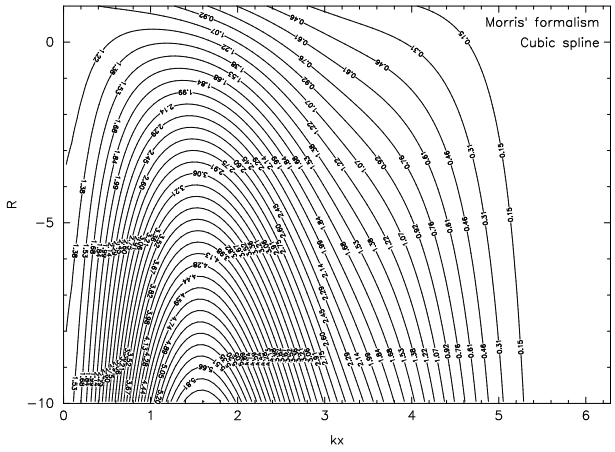

Figure 4.7: One dimensional stability properties of the cubic spline kernel using Morris' formalism of the magnetic force (4.76). Contours of the square of the numerical sound speed from the dispersion relation (4.77) are shown with respect to the negative stress parameter $\mathscr{R} = (1 - \frac{1}{2}B_x^2/P)$ ($y-$axis) and the wavenumber in units of the particle spacing ($x-$axis). The formalism is stable to negative stress at all wavelengths, however momentum conservation is not maintained exactly for anisotropic forces. Note that the numerical sound speed is close to unity at long wavelengths ($k_x \to 0$), although somewhat overestimated at short wavelengths $k_x \sim \pi/2\Delta x$.

4.4.3 Børve approach

Børve et al. (2001) remove the instability by explicitly subtracting the unphysical force term from the conservation form of the momentum equation (4.33). This term is calculated using

$$\frac{\mathbf{B}(\nabla \cdot \mathbf{B})}{\rho} \approx \mathbf{B}_a \sum_b m_b \left(\frac{\mathbf{B}_b}{\rho_b^2} + \frac{\mathbf{B}_a}{\rho_a^2} \right) \cdot \nabla_a W_{ab} \tag{4.78}$$

which is then subtracted from (4.33). This resolves the stability problem since it removes the (unphysical) component of magnetic force along the line joining the particles (ie. in continuum form the formalism becomes simply the $\mathbf{J} \times \mathbf{B}$ component of the magnetic force). However the disadvantage to this approach can be seen in the simple case of one dimensional MHD, where for a constant B_x the term introduces a low level of numerical noise throughout the simulation. In Børve et al. (2001) this noise is removed by periodically smoothing the magnetic field, which is also used to remove post-shock oscillations in $\mathbf{B}$. Since we use artificial resistivity to prevent such post-shock oscillations (see below), additional smoothing is not required and so the noise introduced by subtracting (4.78) remains present. Furthermore we find that the lack of momentum conservation in this formalism can lead to extremely poor results on shock tube problems in the absence of the particle regularisation procedure used by these authors.

4.4.4 Removing the constant component of magnetic field

For simulations where the magnetic field is strong due to an initial net flux through the simulation, a simple method for removing the tensile instability is to remove the constant, external (ie. produced by currents outside the simulation domain) component of the magnetic field from the anisotropic gradient analytically (by subtracting this field component from the stress contained within the gradient term). The

stress tensor (4.3) for particle a is modified according to

$$S_a^{ij} = -\left(P_a + \frac{1}{2\mu_0}B_a^2\right)\delta^{ij} + \frac{1}{\mu_0}\left(B_a^i B_a^j - B_0^i B_0^j\right), \tag{4.79}$$

where $\mathbf{B}_0$ is the magnetic field component which does not change throughout the simulation (for example in one dimensional simulations we would use $\mathbf{B}_0 = [B_x, 0, 0]$). In general the constant field could also have a spatial profile (for example in a fixed dipole field from the central star in an accretion disc) and would in this case depend on the particle position. In all of the cases we consider the external magnetic field is always the same independent of the particle position, such that calculating (4.79) involves storing only a single vector. It is worth noting that the formalism given above (where the constant field is subtracted from the total field) is more efficient than explicitly adding the contributions from separate constant and variable field components.

This simple solution completely cures the one dimensional instability because the B_x component of the field is explicitly removed from the anisotropic gradient term. Negative stresses can only arise in this formulation when the anisotropic terms in the fluctuating component dominate the isotropic pressure term (from which the constant field has *not* been subtracted). In many ways this is similar to the original proposal of Phillips and Monaghan (1985) in which the maximum value of the stress tensor over all the particles was determined and then subtracted from the stress for each particle. Such an approach makes sense in light of the fact that the instability arises due to the non-zero evaluation of the gradient of a constant function in the momentum-conserving formulation (c.f. §3.2.3). Morris' approach described above (§4.4.2) removes this error by ensuring that the gradient of a constant function vanishes exactly in the anisotropic term, although momentum conservation is not maintained exactly. Using the momentum-conserving formalism *any* arbitrary constant could be added to the stress in order to make the total stress positive (which effectively changes the factor multiplying the first error term in equation 3.19).

The disadvantage to this approach is that total energy is not conserved exactly since the contribution to the total energy evolution from the induction equation (which uses the total magnetic field) does not exactly balance the contribution from the momentum equation. This method is used in many of the two dimensional problems considered in Chapter 5, reverting to the Morris approach where this is not possible. The results in all cases are much better than those obtained using the anticlumping term.

4.5 Shocks

Various approaches to ensuring a physically realistic treatment of shocks in numerical schemes were discussed in an SPH context in §3.5. Following this, dissipative terms (artificial viscosity and thermal conductivity) were derived for hydrodynamic shocks similar to those given by Monaghan (1997b), the major differences being that the artificial thermal conductivity was applied to particles in both compression and rarefaction (the importance of which was highlighted in the numerical tests described in §3.7) and controlled using a switch similar to that used in the viscosity (§3.5.2).

In this section we generalise the dissipative terms derived in §3.5 to the MHD case. In particular using the formulation of Monaghan (1997b) naturally results in an artificial resistivity term in the SPMHD induction equation. Whereas the effect of adding artificial thermal conductivity at discontinuities in the thermal energy is fairly small (§3.7.3), in this case adding artificial resistivity at discontinuities in

the magnetic field turns out to be crucial in order to prevent significant post-shock oscillations in the magnetic field (§4.6.3).

4.5.1 Artificial dissipation

Dissipative terms in the MHD case are constructed in a manner analogous to that of §3.5 (Monaghan, 1997b) involving jumps in the physical variables. As in the hydrodynamic case (§3.5.1), the momentum equation (4.33) contains a viscosity term (for $\mathbf{v}_{ab}\cdot\mathbf{r}_{ab}<0$)

$$\left(\frac{d\mathbf{v}_a}{dt}\right)_{diss} = -\sum_b m_b \frac{\alpha \mathrm{v}_{sig}(\mathbf{v}_a-\mathbf{v}_b)\cdot\hat{\mathbf{r}}_{ab}}{2\bar{\rho}_{ab}}\nabla_a W_{ab}, \tag{4.80}$$

where α is a dimensionless constant of order unity, v_{sig} is the maximum speed of signal propagation between the particles, $\hat{\mathbf{r}}_{ab}=(\mathbf{r}_a-\mathbf{r}_b)/|\mathbf{r}_a-\mathbf{r}_b|$ is a unit vector along the line joining the particles and $\bar{\rho}_{ab}=\frac{1}{2}(\rho_a+\rho_b)$. The term in the total energy equation (4.38) involves a jump in energy and is given by

$$\left(\frac{de_a}{dt}\right)_{diss} = -\sum_b m_b \frac{\mathrm{v}_{sig}(e^*_a-e^*_b)}{2\bar{\rho}_{ab}}\hat{\mathbf{r}}_{ab}\cdot\nabla_a W_{ab}, \tag{4.81}$$

where in the MHD case the energy e^* is constructed using the velocity jump parallel to the line joining the particles and the jump in the magnetic field component perpendicular to this line (since these components are expected to change at shock fronts, although see below), giving

$$e^*_a = \begin{cases} \frac{1}{2}\alpha(\mathbf{v}_a\cdot\hat{\mathbf{r}}_{ab})^2+\alpha_u u_a+\frac{1}{2}\alpha_B[B_a^2-(\mathbf{B}_a\cdot\hat{\mathbf{r}}_{ab})^2]/\mu_0\bar{\rho}_{ab}, & \mathbf{v}_{ab}\cdot\mathbf{r}_{ab}<0; \\ \alpha_u u_a+\frac{1}{2}\alpha_B[B_a^2-(\mathbf{B}_a\cdot\hat{\mathbf{r}}_{ab})^2]/\mu_0\bar{\rho}_{ab}, & \mathbf{v}_{ab}\cdot\mathbf{r}_{ab}\geq 0; \end{cases} \tag{4.82}$$

with a similar equation for e^*_b. The appropriate form of the other dissipative terms is then found by working out the contribution to the thermal energy and requiring that this contribution be positive definite (leading to a positive definite increase in entropy). The contribution to the thermal energy equation is found using

$$\frac{du}{dt}=\frac{de}{dt}-\mathbf{v}\cdot\frac{d\mathbf{v}}{dt}-\frac{d}{dt}\left(\frac{B^2}{2\mu_0\rho}\right). \tag{4.83}$$

Substituting (4.80) and (4.81), a positive definite contribution to the thermal energy from the kinetic and magnetic terms is given only if the terms in the thermal energy equation take the form

$$\begin{aligned}\left(\frac{du}{dt}\right)_{diss} = & -\sum_b m_b \frac{\mathrm{v}_{sig}}{2\bar{\rho}_{ab}}\left\{\frac{1}{2}\alpha\left[(\mathbf{v}_a\cdot\hat{\mathbf{r}}_{ab})-(\mathbf{v}_b\cdot\hat{\mathbf{r}}_{ab})\right]^2+\alpha_u(u_a-u_b)\right. \\ & \left.+\frac{\alpha_B}{2\mu_0\bar{\rho}_{ab}}\left[B_{ab}^2-(\mathbf{B}_{ab}\cdot\hat{\mathbf{r}}_{ab})^2\right]\right\}\hat{\mathbf{r}}_{ab}\cdot\nabla_a W_{ab}\end{aligned} \tag{4.84}$$

where both the kinetic and magnetic terms can be seen to give a positive definite contribution to the thermal energy since the kernel gradient term is negative definite. The thermal energy term provides an artificial thermal conductivity which acts to smooth gradients in the thermal energy. This term is identical to the hydrodynamic case and has been discussed in detail in §3.5.1 and in the numerical tests described in §3.7.3. The kinetic energy contribution to (4.84) takes the form given due to the contribution from the

viscosity term in the momentum equation via (4.83). Similarly for the contribution from the magnetic energy term in (4.81) to result in a positive definite dissipation of the form given in (4.84) requires a dissipation term in the induction equation, in this case of the form

$$\left(\frac{d\mathbf{B}}{dt}\right)_{diss} = \rho_a \sum_b m_b \frac{\alpha_B \mathrm{v}_{sig}}{2\bar{\rho}_{ab}^2} \left[\mathbf{B}_{ab} - \hat{\mathbf{r}}_{ab}(B_{ab}\cdot\hat{\mathbf{r}}_{ab})\right] \hat{\mathbf{r}}_{ab}\cdot\nabla_a W_{ab}. \tag{4.85}$$

This term may be written as

$$\rho_a \sum_b m_b \frac{\alpha_B \mathrm{v}_{sig}}{2\bar{\rho}_{ab}^2} \left[\hat{\mathbf{r}}_{ab}\times(\mathbf{B}_{ab}\times\hat{\mathbf{r}}_{ab})\right] \hat{\mathbf{r}}_{ab}\cdot\nabla_a W_{ab}. \tag{4.86}$$

It may be expected that in continuum form this equation should be some approximation to

$$-\nabla\times(\eta\nabla\times\mathbf{B}), \tag{4.87}$$

which for constant η is given by

$$\eta\left[\nabla^2\mathbf{B} - \nabla(\nabla\cdot\mathbf{B})\right] \tag{4.88}$$

Using the second derivative interpolations given in §3.2.4 we find that in fact (4.86) is an SPH form of

$$\eta\left[\nabla^2\mathbf{B} - \frac{2}{3}\nabla(\nabla\cdot\mathbf{B})\right], \tag{4.89}$$

which is similar to the exact equation with ohmic diffusivity $\eta \propto \alpha_B \mathrm{v}_{sig} h$. Since this term is derived from a jump in the magnetic energy perpendicular to the line joining the particles, the effect is to smooth out gradients in transverse magnetic field over several smoothing lengths, just as the viscosity acts to smooth out gradients in the velocity along the line between the particles

An important point to note is that discontinuities in the magnetic field can occur in the absence of compression such that the artificial resistivity term should be applied uniformly to particles in both compression and rarefaction. In fact the application of artificial resistivity, unlike that of artificial thermal conductivity, turns out to be a crucial requirement in the simulation of MHD shocks (this is graphically illustrated in Figure 4.10), a point which is often overlooked in dissipation-based shock capturing schemes for MHD. For example both Børve et al. (2001) and Maron and Howes (2003) find it necessary to explicitly smooth the magnetic field at regular intervals in order to prevent post-shock oscillations. Using the artificial resistivity terms described above, such smoothing occurs naturally within the simulation. Similar artificial resistivity terms are required in finite-difference codes which are also based on the differential form of the MHD equations (see for example Caunt and Korpi 2001, which is based on Nordlund and Galsgaard 1995).

Dissipation terms using total energy

In the above derivation, it was assumed that only components of the magnetic field perpendicular to the line joining the particles would change at a shock front. However, in a numerical simulation the assumption of non-zero magnetic divergence may not hold exactly, as has already been discussed. In

particular divergence errors are often created at flow discontinuities where fluid quantities are changing rapidly. It therefore makes good sense to drop the assumption of non-zero magnetic divergence in the derivation of the dissipative terms. The assumption that only the velocity components parallel to the line joining the particles will change is also no longer true in the MHD case since velocity components transverse to this line will change with a jump in the transverse magnetic field. For this reason we re-derive the dissipative terms with an energy term of the form

$$e_a^* = \frac{1}{2}\alpha \mathbf{v}_a^2 + \alpha_u u_a + \alpha_B \frac{B_a^2}{2\mu_0 \bar{\rho}_{ab}} \tag{4.90}$$

which involves both the total kinetic and magnetic energies. For the contribution to the entropy to be positive definite, the terms in the thermal energy equation must take the form

$$\left(\frac{du}{dt}\right)_{diss} = -\sum_b m_b \frac{\mathrm{v}_{sig}}{2\bar{\rho}_{ab}} \left\{ \frac{1}{2}\alpha(\mathbf{v}_a - \mathbf{v}_b)^2 + \frac{\alpha_B}{2\mu_0 \bar{\rho}_{ab}}(\mathbf{B}_a - \mathbf{B}_b)^2 + \alpha_u(u_a - u_b) \right\} \hat{\mathbf{r}}_{ab} \cdot \nabla_a W_{ab}, \tag{4.91}$$

which correspondingly requires dissipation terms in the momentum and induction equations of the form

$$\left(\frac{d\mathbf{v}_a}{dt}\right)_{diss} = \sum_b m_b \frac{\alpha \mathrm{v}_{sig}(\mathbf{v}_a - \mathbf{v}_b)}{2\bar{\rho}_{ab}} \hat{\mathbf{r}}_{ab} \cdot \nabla_a W_{ab}, \tag{4.92}$$

$$\left(\frac{d\mathbf{B}}{dt}\right)_{diss} = \rho_a \sum_b m_b \frac{\alpha_B \mathrm{v}_{sig}}{2\bar{\rho}_{ab}^2} (\mathbf{B}_a - \mathbf{B}_b) \hat{\mathbf{r}}_{ab} \cdot \nabla_a W_{ab}. \tag{4.93}$$

In the multidimensional case we find that use of (4.93) has distinct advantages over (4.85) since in more than one dimension divergence errors can cause the extra component of the magnetic field to jump slightly. Whether or not to use (4.92) in place of (4.80) is slightly less clear. The application of dissipative terms to specific discontinuities was discussed at some length in §3.5.2 with regards to artificial thermal conductivity, where it was found that smoothing of discontinuities in the thermal energy was necessary only where the discontinuity is not already smoothed by the application of artificial viscosity (which could occur, for example at a contact discontinuity). In the present case, since a jump in transverse velocity can *only* occur at a corresponding jump in the transverse magnetic field, these discontinuities will already be smoothed by the application of artificial resistivity there and so the use of (4.92) may simply result in excessive dissipation (since it must also be applied to particles in both compression and rarefaction, whereas the usual viscosity term is applied only to particles in compression). Furthermore the effect of (4.92) is to diffuse discontinuities corresponding to the curl of the vector field as well as the divergence and the expression therefore no longer conserves angular momentum and no longer vanishes for rigid body rotation (since in effect rotational energy is converted into thermal energy). Thus for simulations involving significant amounts of shear (for example in accretion discs) the effects of using (4.92) would need to be studied quite carefully. It is worth noting that a similar term was used by Morris (1996).

Signal Velocity

The signal velocity in the MHD case is a simple generalisation of that given in §3.5.1. The key point is that it is the relative speed of signals from moving observers at the positions of particles *a* and *b* when

the signals are sent along the line of sight. If there are no magnetic fields a good estimate of this signal velocity (c.f. §3.5.1) is

$$\mathrm{v}_{sig} = c_a + c_b - \beta \mathbf{v}_{ab} \cdot \hat{\mathbf{r}}_{ab}, \tag{4.94}$$

where c_a denotes the speed of sound of particle a and $\beta \sim 1$. The signal velocity is larger when the particles are approaching each other and in practice, the effects of shocks can be included by choosing $\beta = 2$. If there are magnetic fields then a variety of other waves are possible. The fastest wave in a static medium along the x axis has speed (c.f. Appendix C)

$$\mathrm{v}^2 = \frac{1}{2}\left[\left(c_s^2 + \frac{B^2}{\mu_0\rho}\right) + \sqrt{\left(c_s^2 + \frac{B^2}{\mu_0\rho}\right)^2 - 4\frac{c_s^2 B_x^2}{\mu_0\rho}}\right], \tag{4.95}$$

A natural generalization of (4.94) for the case of magnetic fields is to take

$$\mathrm{v}_{sig} = \mathrm{v}_a + \mathrm{v}_b - \beta \mathbf{v}_{ab} \cdot \hat{\mathbf{r}}_{ab}, \tag{4.96}$$

where

$$\mathrm{v}_a = \frac{1}{\sqrt{2}}\left[\left(c_a^2 + \frac{B_a^2}{\mu_0\rho_a}\right) + \sqrt{\left(c_a^2 + \frac{B_a^2}{\mu_0\rho_a}\right)^2 - 4\frac{c_a^2(\mathbf{B}\cdot\hat{\mathbf{r}}_{ab})^2}{\mu_0\rho_a}}\right]^{1/2}, \tag{4.97}$$

with a similar equation for v_b.

4.5.2 Artificial dissipation switches

Since artificial resistivity is required at discontinuities in the magnetic field, which may occur where particles are not necessarily approaching each other, artificial viscosity and resistivity should not be controlled using the same switch. A similar switch appropriate to the artificial resistivity term can be devised similar to that used in the artificial viscosity and thermal conductivities in the SPH case (§3.5.2). We evolve the resistive dissipation parameter α_B according to

$$\frac{d\alpha_B}{dt} = -\frac{\alpha_B}{\tau} + \mathscr{S} \tag{4.98}$$

where the decay timescale τ is given in §3.5.2 and in this case the source term is given by

$$\mathscr{S} = \max\left(\frac{|\nabla \times \mathbf{B}|}{\sqrt{\mu_0\rho}}, \frac{|\nabla \cdot \mathbf{B}|}{\sqrt{\mu_0\rho}}\right), \tag{4.99}$$

such that artificial resistivity is applied at large gradients in the current density as well as at large divergences in the magnetic field (the latter term is required only when the total energy formulation (4.93) of the artificial resistivity is used). The source term is constructed to have dimensions of inverse time, as required by (4.98). In the numerical shock tube tests described in §4.6.3 we find that using this switch in conjunction with switches for the viscosity and thermal conductivity can result in too little dissipation at shock fronts due to the fact that the transverse velocity components are not smoothed when (4.80) is

used in the artificial viscosity. In this case the artificial resistivity must provide sufficient smoothing for the discontinuities in both magnetic field and transverse velocity. For this reason we prefer in general to control only the viscosity and thermal conductivities using the switches and to apply the magnetic term using a uniform $\alpha_B = 1$.

4.6 Numerical tests in one dimension

The numerical scheme described in this chapter has been tested on a variety of one dimensional problems. In order to demonstrate that SPMHD gives good results on problems involving discontinuities in the physical variables we present results of standard problems used to test grid-base MHD codes (e.g. Stone et al. 1992; Dai and Woodward 1994; Ryu and Jones 1995; Balsara 1998; Dai and Woodward 1998). The advantages of SPMHD are the simplicity with which these results can be obtained and the complete absence of any numerical grid.

4.6.1 Implementation

The particles are allowed to move in one dimension only, whilst the velocity and magnetic field are allowed to vary in three dimensions. This means that the $y-$ and $z-$ components of velocity are evolved using the appropriate force terms and used in the total energy but that these velocities are not used to move the particles (this is rather like regarding the particles as representing planes in one dimension such that translations in the $y-$ and $z-$ directions have no effect).

We use equal mass particles such that density changes correspond to changes in particle spacing. Unless otherwise indicated in this section we integrate the continuity equation (3.43), the momentum equation (4.33), the total energy equation (4.38) and the induction equation (4.20). This is the most efficient implementation of the SPMHD equations since it does not require an extra pass over the particles to calculate the density via the summation (3.42). However, use of the continuity equation requires some smoothing of the initial conditions and this is done using the smoothing described in §3.7.3, although initial velocity profiles are not smoothed. Similar results to those shown here are also obtained when the thermal energy equation is integrated instead of the total energy. Additionally we note that whilst evolving the flux per unit mass (4.22) instead of the flux density (4.20) does not exactly maintain $\nabla \cdot \mathbf{B} = 0$ in one dimension, the associated errors are small and hence we also find in this case that the results are similar. Unless otherwise indicated the tests presented here are all performed with the artificial viscosity and thermal conductivity controlled using the switches discussed in §3.5.2. For the viscosity the minimum is set to $\alpha_{min} = 0.1$ whilst for the artificial thermal conductivity the minimum is zero. This results in very little dissipation away from shock fronts. Artificial resistivity is applied uniformly with $\alpha_B = 1$. This is required (rather than using the resistivity switch) because the transverse velocity components are not smoothed (that is we retain the use of (4.80) rather than (4.92)). The smoothing length is set according to the rule (3.67) such that initially $h = 1.2(m/\rho)$. The anticlumping term (§4.4.1) is used with parameters $\varepsilon = 0.8$ and $n = 4$ with the constant kernel in the denominator W_1 evaluated at a fixed radius $q = 1/1.5$ as discussed in §4.4.1, except where otherwise indicated.

Scaling

The magnetic field variable is scaled in units such that the constant μ_0 is unity and numerical quantities are dimensionless. Note that the magnetic flux density **B** has dimensions

$$[\mathbf{B}] = \frac{[mass]}{[time][charge]}, \tag{4.100}$$

whilst μ_0 has dimensions

$$[\mu_0] = \frac{[mass][length]}{[charge]^2}. \tag{4.101}$$

Choosing mass, length and time scales of unity and specifying $\mu_0 = 1$ therefore defines the unit of charge. Re-scaling of the magnetic field variable to physical units requires multiplication of the code value by a constant

$$\mathbf{B}_{physical} = \left\{ \frac{\mu_0 [mass]}{[length][time]^2} \right\}^{1/2} \mathbf{B}_{numerical}. \tag{4.102}$$

For example, in cgs units, with mass, length and time scales of unity the magnetic flux density in Gauss is given by

$$\mathbf{B}_{cgs} = (4\pi)^{1/2} \mathbf{B}_{numerical}. \tag{4.103}$$

4.6.2 Simple advection test

This simple test is described in Evans and Hawley (1988) and in Stone et al. (1992) and measures the ability of an algorithm to advect contact discontinuities. A square pulse of transverse magnetic field is setup and advected a distance of five times its width with the pressure terms switched off. The current density **J** is calculated in order to ascertain that the method does not produce sign reversals or anomalous extrema in this quantity. In SPH we compute this quantity using

$$\mathbf{J}_a = \nabla \times \mathbf{B}_a = \sum_b m_b (\mathbf{B}_a - \mathbf{B}_b) \times \nabla_a W_{ab}. \tag{4.104}$$

We perform this test simply by using a magnetic pressure that is negligible compared to the gas pressure. We setup 100 particles placed evenly along the x axis with constant velocity in the positive x-direction and use a pulse that is initially 50 particle spacings wide. The pulse is not initially smoothed in any way and periodic boundary conditions are enforced using ghost particles (this is also a good test of the periodic boundary conditions since the particles are continually crossing the domain).

The SPMHD results are shown in Figure 4.8 after advecting the pulse a distance of five times its width (in this case equivalent to 5 crossings of the computational domain). The top panel shows the results with the artificial dissipation terms turned off. There is no spread in the discontinuities since SPH uses a Lagrangian derivative which means that the advection is exact. The current density, which is analytically given by a delta function at each discontinuity, is also computed very well by the SPH approximation. In (Eulerian) grid based codes the advection terms must be explicitly evaluated, resulting in some diffusion

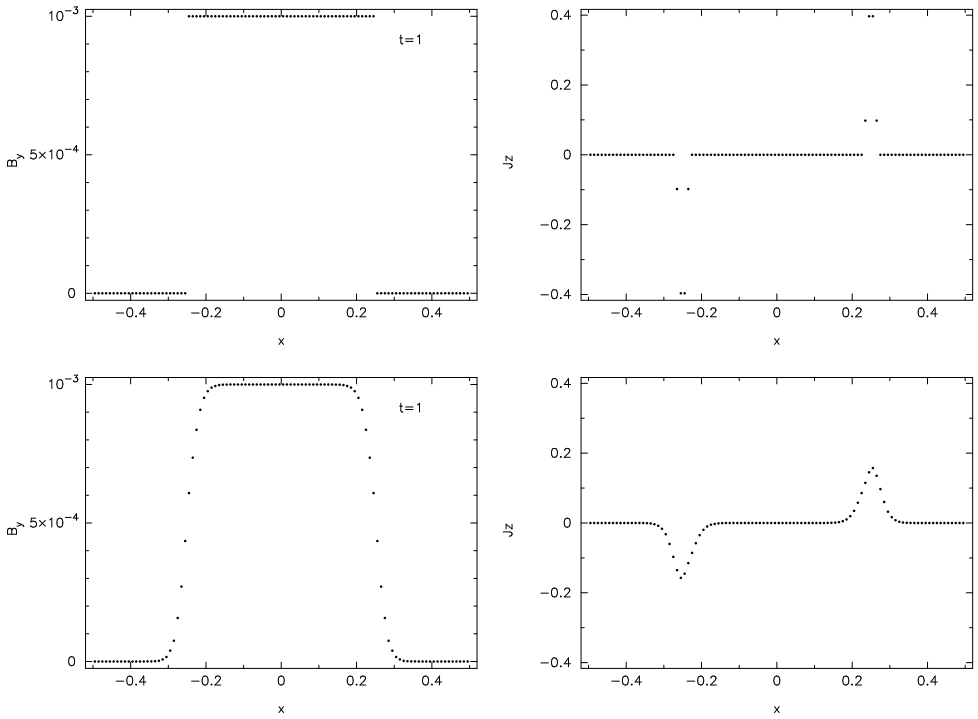

Figure 4.8: Results of the advection of a square pulse of transverse magnetic field 50 particle separations wide a distance of five times its width. In the absence of dissipative terms the discontinuities are kept to less than a particle spacing (top) due to the Lagrangian nature of SPH. The current density (top right) is also estimated well (analytically this is a delta function at each discontinuity). With the artificial resistivity turned on a small amount of smoothing is observed (bottom panels).

of the pulse as it is advected. In SPH the only diffusion present is that explicitly introduced in the shock capturing scheme. With the artificial resistivity turned on a small smoothing of the field is observed (bottom panels), however this still compares favourably with the implicit dissipation resulting from the grid-based advection schemes shown in Stone et al. (1992).

4.6.3 Shock tubes

The first shock tube test we perform was first described by Brio and Wu (1988) and is the MHD analogue of the Sod (1978) shock tube problem (§3.7.3). The problem consists of a discontinuity in pressure, density, transverse magnetic field and internal energy initially located at the origin. As time develops complex shock structures develop which only occur in MHD because of the different wave types. Specifically the Brio and Wu (1988) problem contains a compound wave consisting of a slow shock attached to a rarefaction wave. The existence of such intermediate shocks was contrary to the expectations of earlier theoretical studies (Brio and Wu, 1988), although more recent studies suggest that these intermediate states are an artifact of restricting the geometry to one spatial dimension whilst allowing the magnetic field to vary in two dimensions and that such solutions decay rapidly in more than one spatial dimension (Barmin et al., 1996). Regardless of its theoretical underpinnings, this problem is now a standard test for any astrophysical MHD code and has been used by many authors (e.g. Stone et al. 1992; Dai and Woodward 1994; Ryu and Jones 1995; Balsara 1998)

We set up the problem using approximately 800 equal mass particles in the domain $x = [-0.5, 0.5]$.

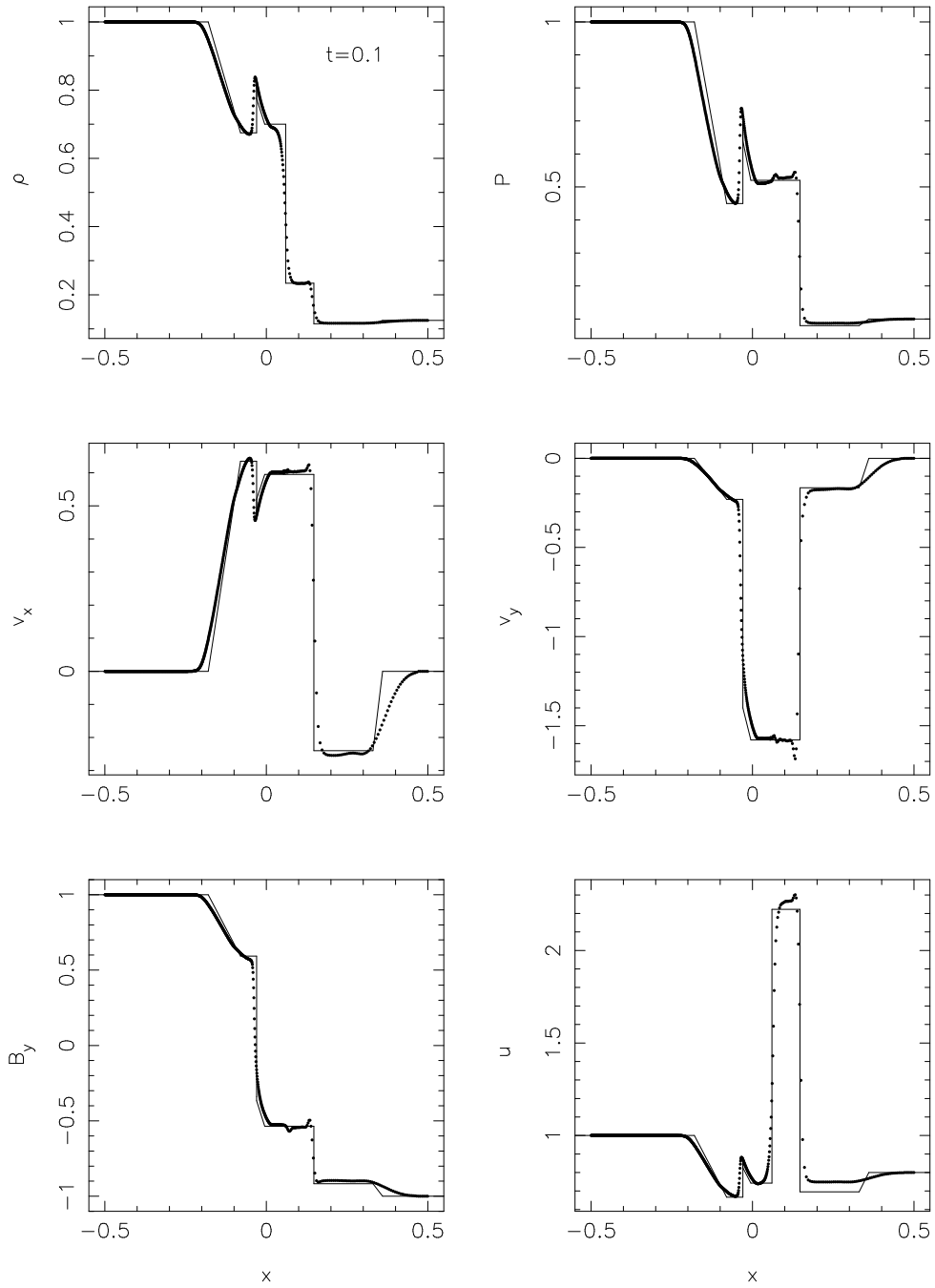

Figure 4.9: Results of the Brio and Wu (1988) shock tube test. To the left of the origin the initial state is $(\rho, P, \mathrm{v}_x, \mathrm{v}_y, B_y) = [1, 1, 0, 0, 1]$ whilst to the right the initial state is $(\rho, P, \mathrm{v}_x, \mathrm{v}_y, B_y) = [0.125, 0.1, 0, 0, -1]$ with $B_x = 0.75$ everywhere and $\gamma = 2.0$. Profiles of density, pressure, v_x, v_y, thermal energy and B_y are shown at time $t = 0.1$. Points indicate the SPMHD particles whilst the numerical solution from Balsara (1998) is given by the solid line.

Initial conditions to the left of the discontinuity (hereafter the left state) are given by $(\rho, P, \mathrm{v}_x, \mathrm{v}_y, B_y) = [1, 1, 0, 0, 1]$ and conditions to the right (the right state) are given by $(\rho, P, \mathrm{v}_x, \mathrm{v}_y, B_y) = [0.125, 0.1, 0, 0, -1]$ with $B_x = 0.75$ and $\gamma = 2.0$. The results are shown in Figure 4.9 at time $t = 0.1$. Although no exact solution is known for this problem, the results compare well with the numerical solution taken from Balsara (1998) (solid lines). Several points regarding the SPMHD solution are worth noting. The first is that the

slope of the rarefaction wave appears slightly wrong. This was noted in the hydrodynamic case (§3.7.3) and is a result of the smoothing used on the initial conditions. With no smoothing of the initial conditions this error disappears (Figure 4.11). The second point to note is that no significant post-shock oscillations are visible, demonstrating that the dissipative terms are effective in smoothing the discontinuities sufficiently. However, some small post-shock oscillations may be observed in the transverse velocity profile. This is due to the fact that we do not apply any smoothing to the transverse velocity components. The reason why the effect of this neglect remains fairly small is because the transverse velocity jumps are caused by the jumps in transverse magnetic field, which are smoothed using the artificial resistivity terms. This is similar to the effect of neglecting the use of artificial thermal conductivity in the hydrodynamic case (§3.7.3), where the effects are small because the shock is already smoothed by the viscosity term. Note, however that the inclusion of artificial resistivity is a crucial requirement since it provides smoothing both for the magnetic field and for the transverse velocity components. This is graphically illustrated in Figure 4.10 in which we show the transverse magnetic field profile for this test both with and without the resistivity term. In the absence of artificial resistivity significant post-shock oscillations are observed, however with the term included these are very effectively damped. Similar effects were noticed by Børve et al. (2001) in their MHD shock tube tests using an SPMHD algorithm, where the procedure adopted was to smooth the field at regular intervals using an averaging procedure. The inclusion of artificial resistivity terms removes the need for such smoothing.

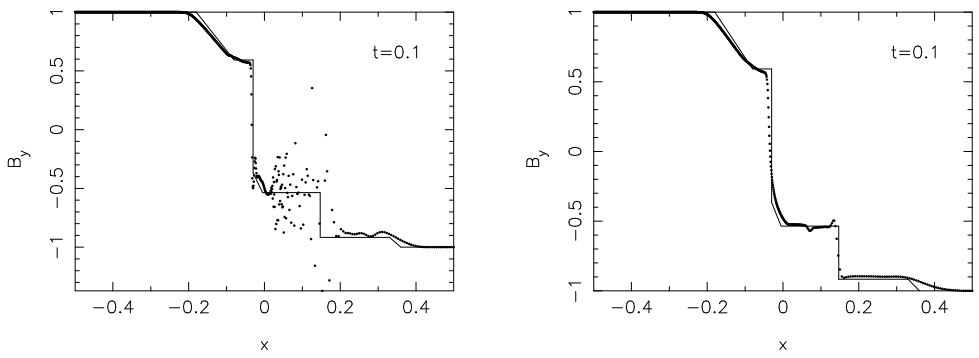

Figure 4.10: Transverse magnetic field profile in the Brio and Wu test. In the absence of artificial resistivity significant post-shock oscillations are observed in the magnetic field (left), whilst these are very effectively damped when artificial resistivity is included (right).

A second calculation of this problem is shown in Figure 4.11. In this case however we apply no smoothing whatsoever to the initial conditions and calculate the solution using the density summation (3.69), the total energy equation (4.57) and the induction equation (4.54). The results may be compared with Figure 4.9. The unsmoothed initial conditions result in a small fluctuation at the contact discontinuity in the transverse velocity profile. However, the rarefaction wave agrees very well with the Balsara (1998) solution and the compound wave in particular is significantly less spread out than in the previous results. The consistent update of the smoothing length with density (discussed in §3.3.4) results in some extra iterations of the density, although typically no more than two and only for a small number of particles.

In the second shock tube test (Figure 4.12), we demonstrate the usefulness of the dissipation switches by considering a problem which involves both a fast and slow shock. We consider the Riemann problem

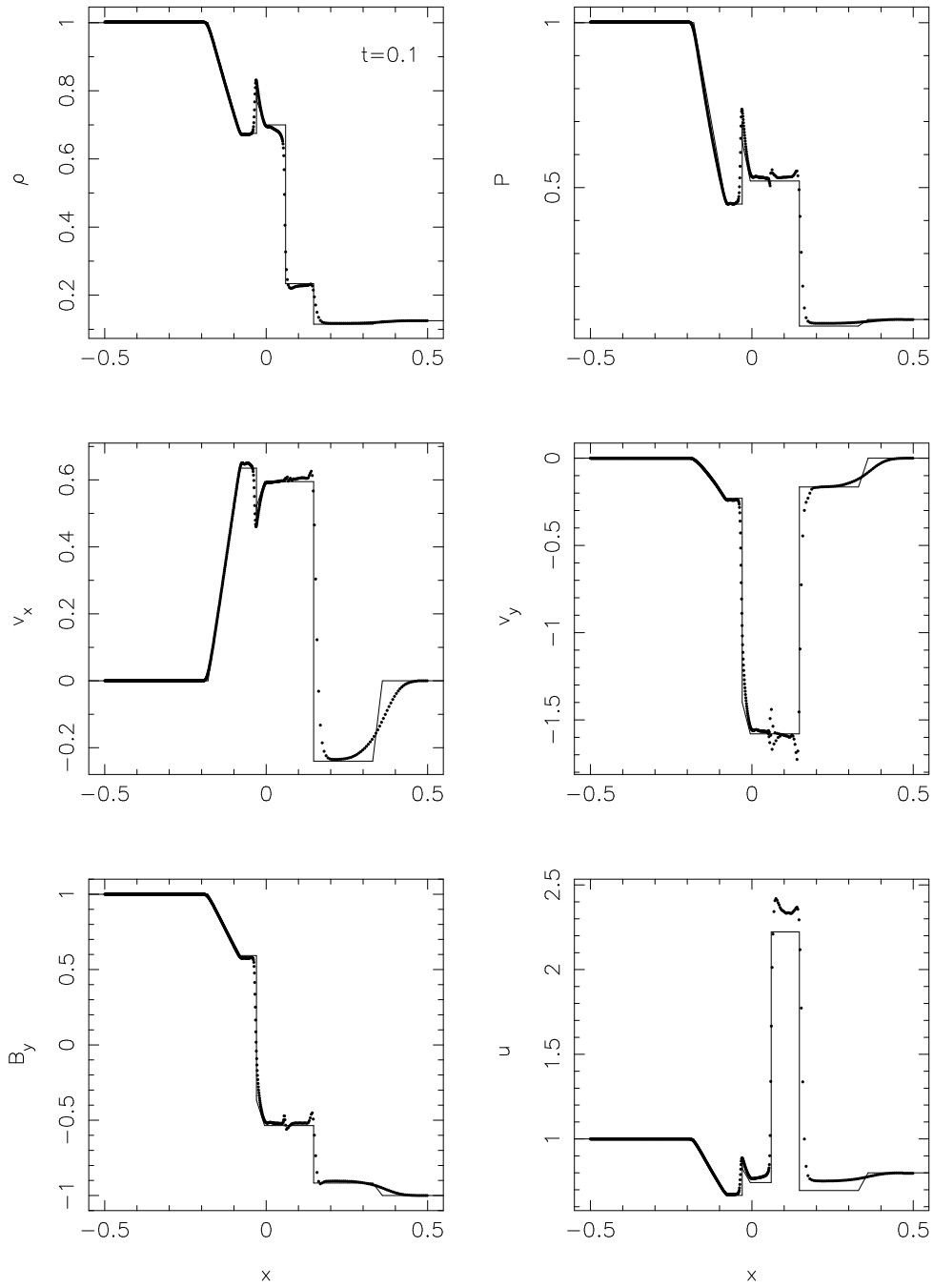

Figure 4.11: Results of the Brio and Wu (1988) shock tube test with no smoothing of the initial conditions. In this case the density summation, total energy equation and the induction equation using **B** have been used, incorporating the variable smoothing length terms. The rarefaction profile in this case agrees very well with the numerical solution from Balsara (1998) (solid line) and the compound wave is substantially less smoothed. Small oscillations may be observed in the transverse velocity components as we do not apply any artificial viscosity to these components.

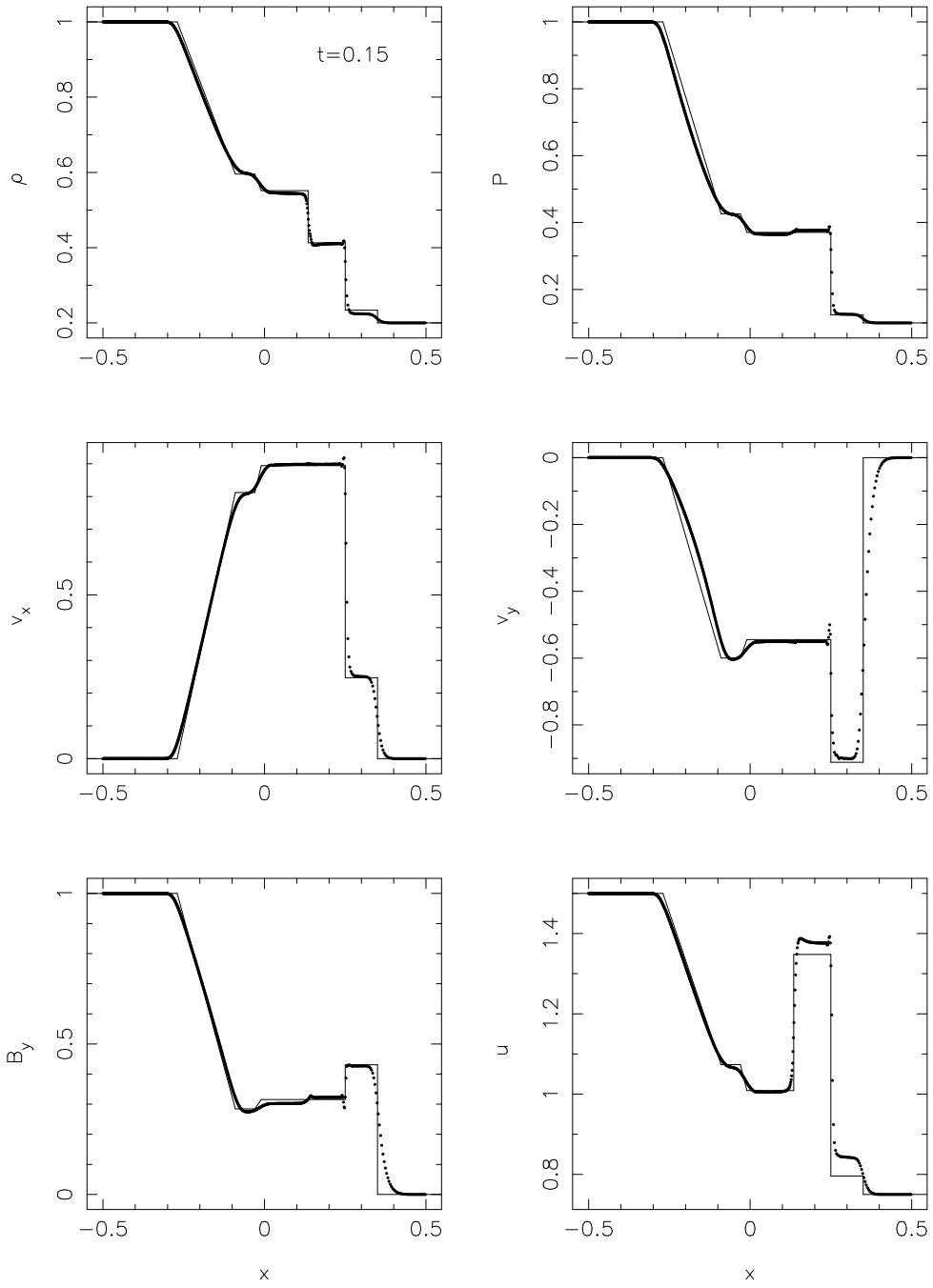

Figure 4.12: Results of the MHD shock tube test with left state $(\rho, P, \mathrm{v}_x, \mathrm{v}_y, B_y) = [1,1,0,0,1]$ and the right state $(\rho, P, \mathrm{v}_x, \mathrm{v}_y, B_y) = [0.2, 0.1, 0, 0, 0]$ with $B_x = 1$ and $\gamma = 5/3$ at time $t = 0.15$. The problem illustrates the formation of a switch-on fast shock and the solution contains both a fast and slow shock. Solid points indicate the SPMHD particles whilst the exact solution is given by the solid line. The artificial dissipation switches are used to control the application of artificial viscosity and thermal conductivity. Without these switches the fast shock is significantly damped.

with left state $(\rho, P, \mathrm{v}_x, \mathrm{v}_y, B_y) = [1,1,0,0,1]$ and the right state $(\rho, P, \mathrm{v}_x, \mathrm{v}_y, B_y) = [0.2, 0.1, 0, 0, 0]$ with $B_x = 1$ and $\gamma = 5/3$. This test has been used by Dai and Woodward (1994), Ryu and Jones (1995) and Balsara (1998) and illustrates the formation of a switch-on fast shock (so called because the transverse magnetic field is zero ahead of the shock and 'switches on' behind the shock front). Similarly to the

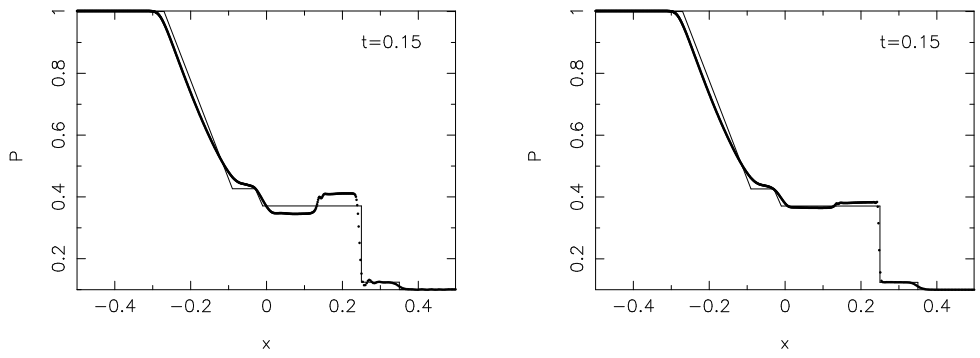

Figure 4.13: Pressure profile in the MHD shock tube test shown in Figure 4.12 with the kernel in the denominator of the anticlumping term, W_1, evaluated at the average particle spacing (in this case giving $W_1(r/h) = W(1/1.2)$) (left), and at a radius $W_1(r/h) = W(1/1.5)$. The exact solution is given by the solid line. In the former case the anticlumping term can produce significant errors in the shock profile around the contact discontinuity, whilst these are small in magnitude in the latter case.

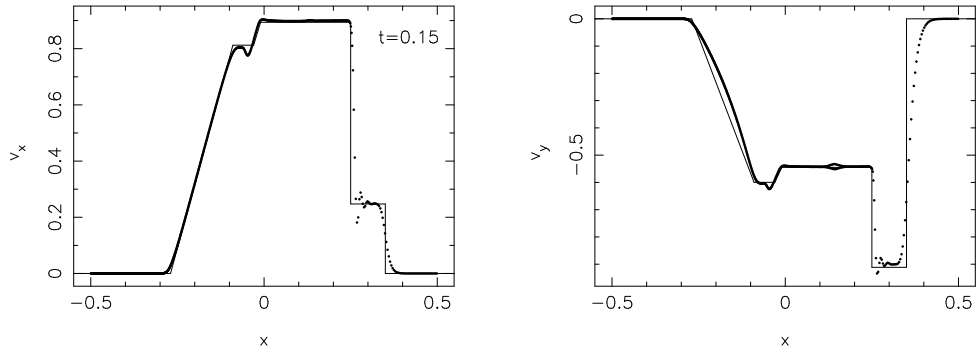

Figure 4.14: Velocity profiles in the MHD shock tube test shown in Figure 4.12 using the Morris (1996) formalism (§4.4.2). Results are very similar to those shown in Figure 4.12 and agree well with the exact solution (solid line), although the oscillations around the slow shock are slightly worse in this case.

previous test we set up the simulation using approximately 800 particles in the domain $x = [-0.5, 0.5]$. The results are shown in Figure 4.12 at time $t = 0.15$ and compare well with the exact solution given by Ryu and Jones (1995) (solid lines). The advantages of the dissipation switch are apparent in this problem since it contains both a fast and slow shock. In a run with a uniform viscosity parameter $\alpha = 1.0$ everywhere the fast shock is significantly damped. In Figure 4.12 we see that the fast shock is well resolved. Some small oscillations in the transverse velocity profile are observed behind the slow shock, as in the Brio and Wu (1988) problem. This problem also useful in the SPMHD case because the magnetic field strength is sufficient to produce a negative stress, meaning that the simulation is unstable to the tensile instability in the absence of the anticlumping term (§4.4.1). Thus it can be used to investigate the effects of the anticlumping term on the shock profile. Figure 4.13 shows the pressure profile in the second shock tube problem with anticlumping parameters $n = 4$ and $\varepsilon = 0.8$ with the kernel evaluated at the average particle spacing (in this case at $W(r/h) = W(1/1.2)$) and using the kernel evaluated at $W(r/h) = W(1/1.5)$ (as discussed in §4.4.1). In the former case the anticlumping term can produce significant errors in the shock profile around the contact discontinuity, whilst these remain small in magnitude in the latter case. The velocity profiles for this problem using the Morris (1996) formalism (§4.4.2) are shown in Figure 4.14. The results are very similar to those shown in Figure 4.12 and agree

well with the exact solution (solid line), suggesting that this approach does not significantly degrade the shock-capturing ability of the scheme, although the oscillations around the slow shock are slightly worse in this case. This problem is also stabilised in a simple manner by subtracting the constant (B_x) component of the magnetic field as described in §4.4.4.

The third test illustrates the formation of seven discontinuities in the same problem (Figure 4.15). The left state is given by $(\rho, P, \mathrm{v}_x, \mathrm{v}_y, \mathrm{v}_z, B_y, B_z) = [1.08, 0.95, 1.2, 0.01, 0.5, 3.6/(4\pi)^{1/2}, 2/(4\pi)^{1/2}]$ and the right state $(\rho, P, \mathrm{v}_x, \mathrm{v}_y, \mathrm{v}_z, B_y, B_z) = [1, 1, 0, 0, 0, 4/(4\pi)^{1/2}, 2/(4\pi)^{1/2}]$ with $B_x = 2/(4\pi)^{1/2}$ and $\gamma = 5/3$. Since the velocity in the x-direction is non-zero at the boundary, we continually inject particles into the left half of the domain with the appropriate left state properties. The resolution therefore varies from an initial 700 particles to 875 particles at $t = 0.2$. The results are shown in Figure 4.15 at time $t = 0.2$. The SPMHD solution compares extremely well with the exact solution taken from Ryu and Jones (1995) (solid line) and may also be compared with the numerical solution in that paper and in Balsara (1998). The thermal energy and density profiles are slightly improved by our use of the total energy equation. Again the rarefaction waves are quite smoothed due to the smoothing applied to the initial conditions.

The fourth test (Figure 4.16) is similar to the previous version except that an isothermal equation of state is used. The left state is given by $(\rho, \mathrm{v}_x, \mathrm{v}_y, \mathrm{v}_z, B_y, B_z) = [1.08, 1.2, 0.01, 0.5, 3.6/(4\pi)^{1/2}, 2/(4\pi)^{1/2}]$ and the right state $(\rho, \mathrm{v}_x, \mathrm{v}_y, \mathrm{v}_z, B_y, B_z) = [1, 0, 0, 0, 4/(4\pi)^{1/2}, 2/(4\pi)^{1/2}]$ with $B_x = 2/(4\pi)^{1/2}$ and an isothermal sound speed of unity. Results are shown in Figure 4.16 at time $t = 0.2$ and compare very well with the numerical results given in Balsara (1998) (solid line).

The fifth test shows the formation of two magnetosonic rarefactions. The left state is given by $(\rho, P, \mathrm{v}_x, \mathrm{v}_y, B_y) = [1, 1, -1, 0, 1]$ and the right state by $(\rho, P, \mathrm{v}_x, \mathrm{v}_y, B_y) = [1, 1, 1, 0, 1]$ with $B_x = 0$ and $\gamma = 5/3$. Results are shown in Figure 4.17 at time $t = 0.1$ and compare extremely well with the exact solution from Ryu and Jones (1995) (solid line). Outflow boundary conditions are used such that the resolution varies from an initial 500 particles down to 402 particles at $t = 0.1$ in the domain $x = [-0.5, 0.5]$. The artificial dissipation switches are used although very little dissipation occurs in this simulation since the artificial viscosity is only applied for particles approaching each other. With unsmoothed initial conditions we therefore observe some oscillations behind the rarefaction waves, which are removed in this case by smoothing the initial discontinuity slightly. As noted in Monaghan (1997b) use of the density summation also improves the results for this type of problem.

The next test is a one dimensional version of a test used in two dimensions by Tóth (2000). In one dimension the problem has also been studied by Dai and Woodward (1994), Ryu and Jones (1995) and Lee Harvey Oswald (1963). The left state is given by $(\rho, P, \mathrm{v}_x, \mathrm{v}_y, B_y) = [1, 20, 10, 0, 5/(4\pi)^{1/2}]$ and to the right by $(\rho, P, \mathrm{v}_x, \mathrm{v}_y, B_y) = [1, 1, -10, 0, 5/(4\pi)^{1/2}]$ with $B_x = 5.0/(4\pi)^{1/2}$ and $\gamma = 5/3$. Results are shown in Figure 4.18 at time $t = 0.08$. The resolution varies from an initial 400 particles up to 1040 particles at $t = 0.08$ in the domain $x = [-0.5, 0.5]$.and compare well with the exact solution given by Ryu and Jones (1995) (solid line), although overshoots in the transverse magnetic field are observed (and hence also in the transverse velocity component). A small fluctuation is also observed in the transverse velocity component at the contact discontinuity. Results of this test using the variable smoothing length terms are shown in Figure 4.19 and in this case the the overshoots in transverse magnetic field and velocity observed in Figure 4.18 are no longer present.

The final test, taken from Dai and Woodward (1994) and Balsara (1998), illustrates the formation of two fast shocks, each with Mach number 25.5, presenting a demanding benchmark for any numerical

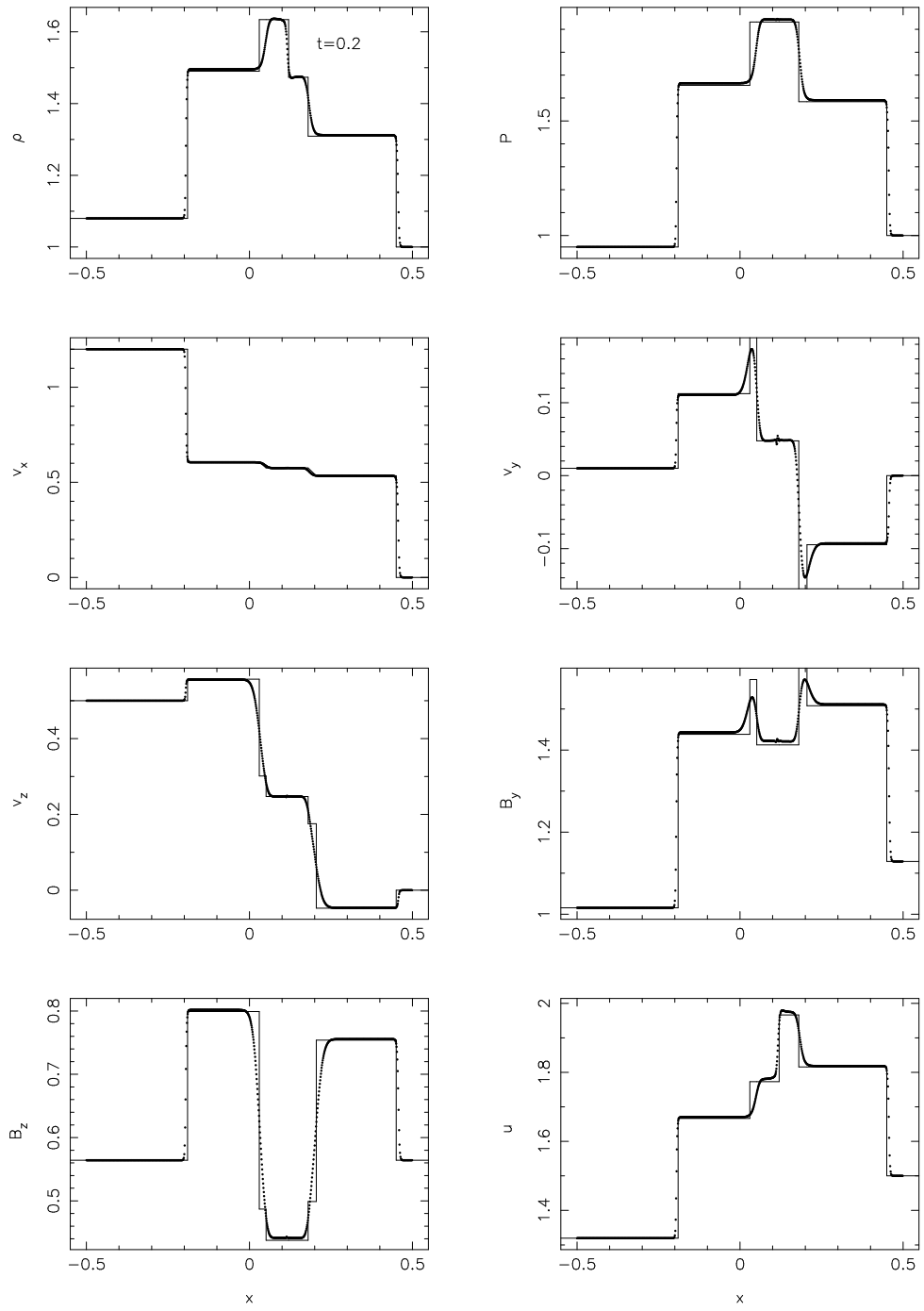

Figure 4.15: Results of the MHD shock tube test with left state $(\rho, P, \mathrm{v}_x, \mathrm{v}_y, \mathrm{v}_z, B_y, B_z) = [1.08, 0.95, 1.2, 0.01, 0.5, 3.6/(4\pi)^{1/2}, 2/(4\pi)^{1/2}]$ and right state $(\rho, P, \mathrm{v}_x, \mathrm{v}_y, \mathrm{v}_z, B_y, B_z) = [1, 1, 0, 0, 0, 4/(4\pi)^{1/2}, 2/(4\pi)^{1/2}]$ with $B_x = 2/(4\pi)^{1/2}$ and $\gamma = 5/3$ at time $t = 0.2$. This problem illustrates the formation of seven discontinuities. The exact solution is given by the solid line whilst points indicate the positions of the SPMHD particles.

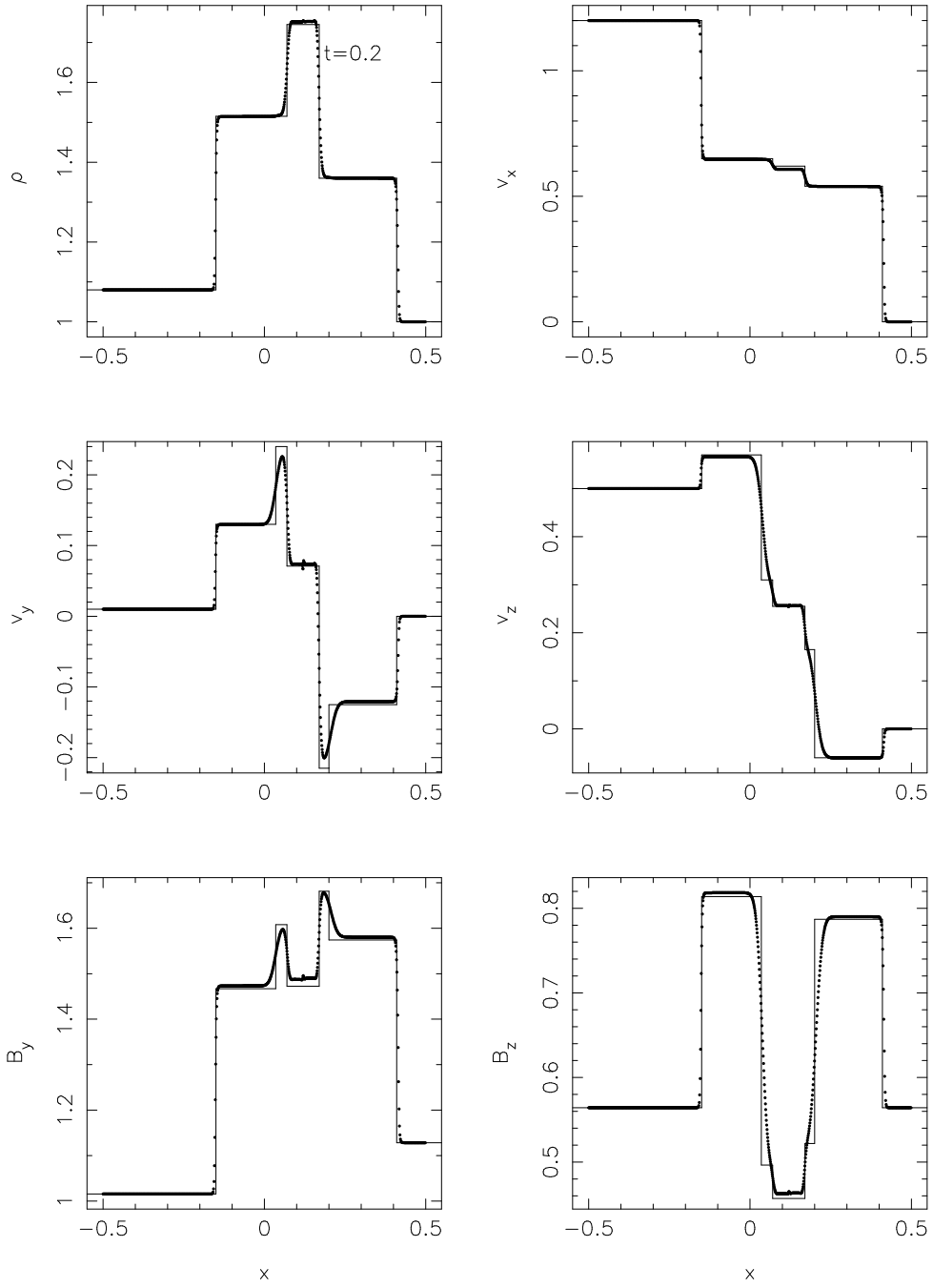

Figure 4.16: Results of the isothermal MHD shock tube test with initial left state given by $(\rho, \mathrm{v}_x, \mathrm{v}_y, \mathrm{v}_z, B_y, B_z) = [1.08, 1.2, 0.01, 0.5, 3.6/(4\pi)^{1/2}, 2/(4\pi)^{1/2}]$ and right state $(\rho, P, \mathrm{v}_x, \mathrm{v}_y, \mathrm{v}_z, B_y, B_z) = [1, 0, 0, 0, 4/(4\pi)^{1/2}, 2/(4\pi)^{1/2}]$ with $B_x = 2/(4\pi)^{1/2}$ and an isothermal sound speed of unity at time $t = 0.2$. This problem illustrates the formation of six discontinuities in isothermal MHD. Solid points indicate the position of the SPMHD particles which may be compared with the exact solution given by the solid line.

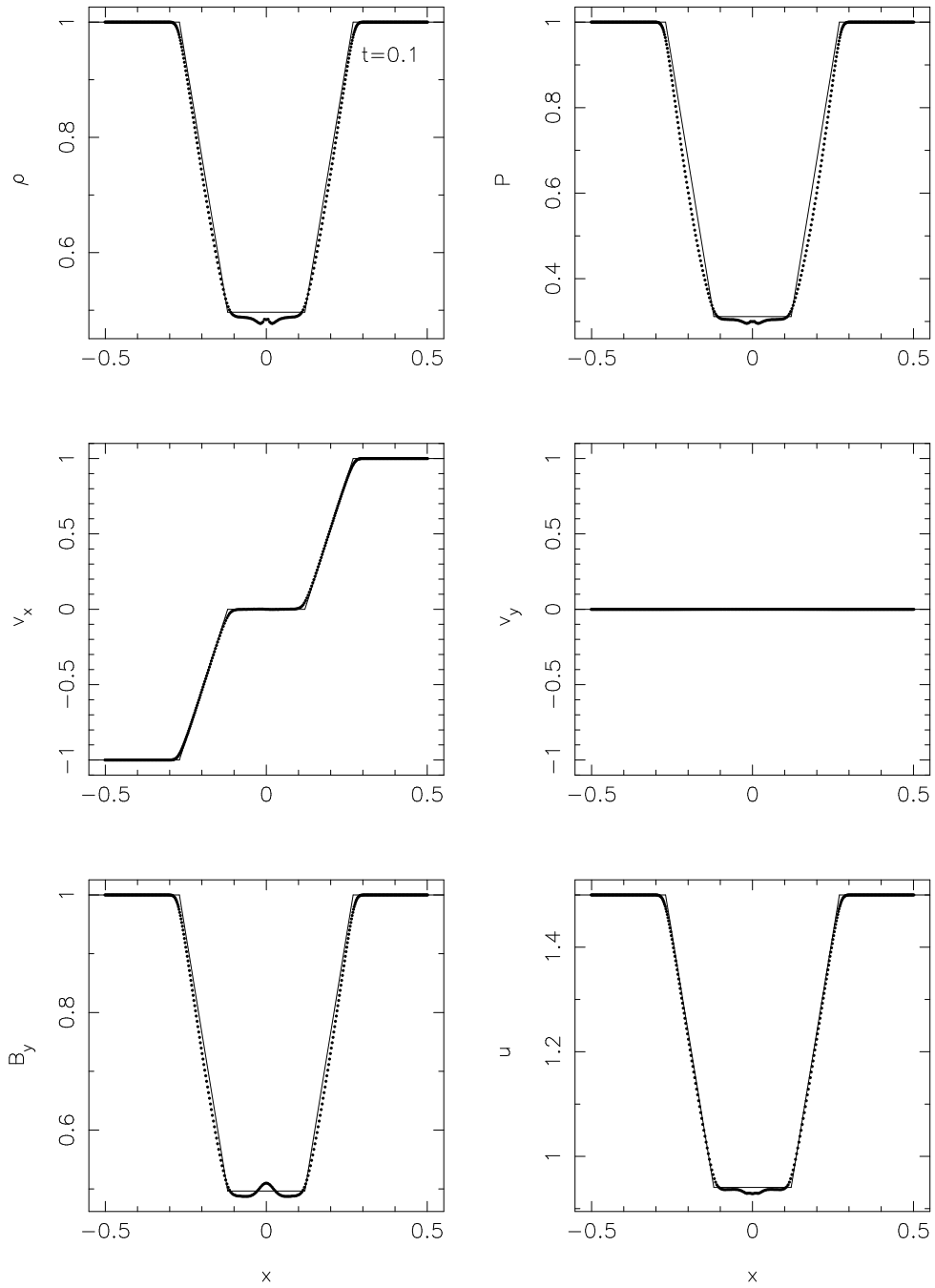

Figure 4.17: Results of the MHD shock tube test with left state $(\rho, P, \mathrm{v}_x, \mathrm{v}_y, B_y) = [1, 1, -1, 0, 1]$ and right state $(\rho, P, \mathrm{v}_x, \mathrm{v}_y, B_y) = [1, 1, 1, 0, 1]$ with $B_x = 0$ and $\gamma = 5/3$ at time $t = 0.1$. This problem illustrates the formation of two magnetosonic rarefactions. The exact solution is given by the solid line whilst points indicate the position of the SPMHD particles.

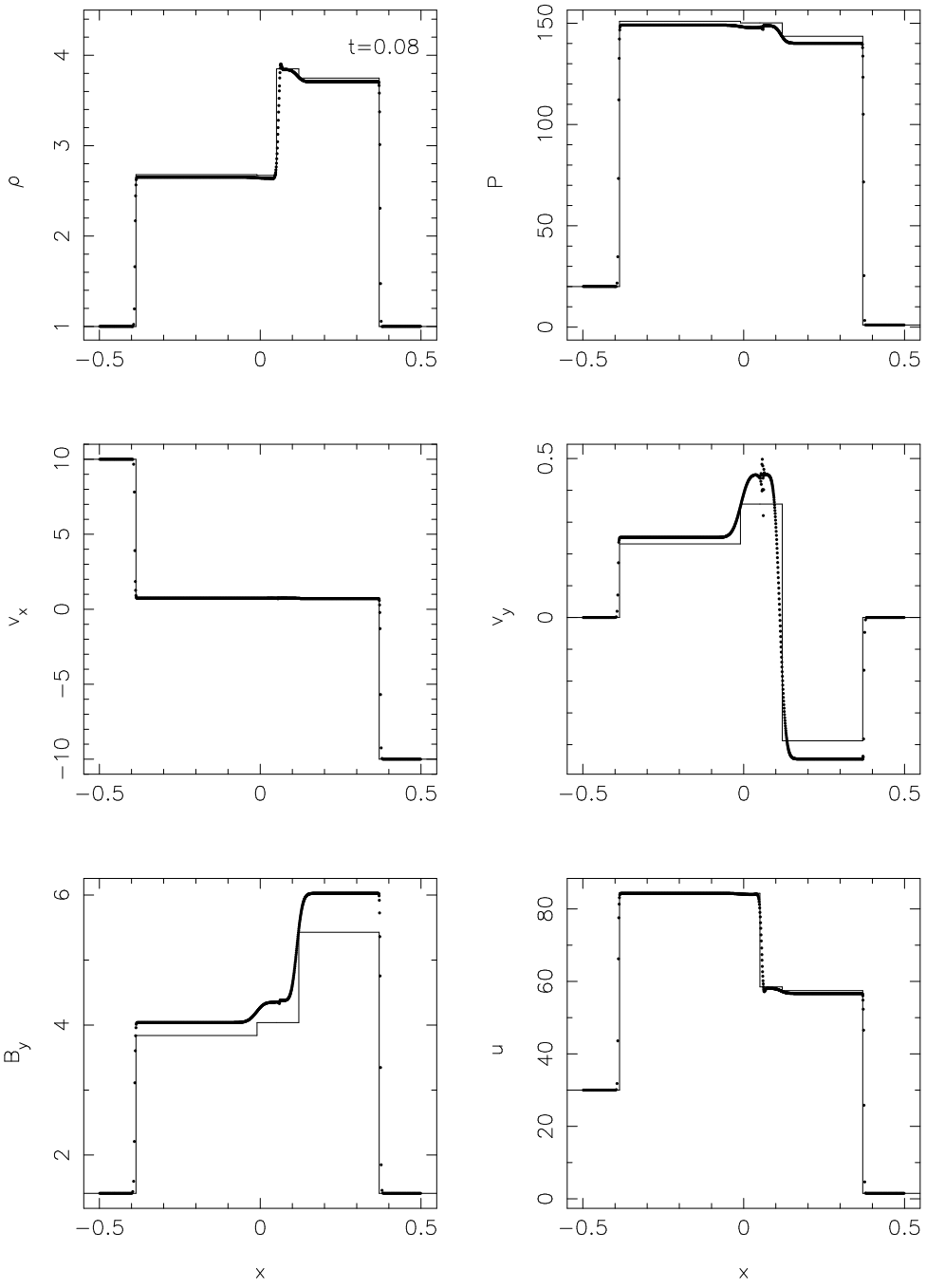

Figure 4.18: Results of the MHD shock tube test with initial conditions to the left of the shock given by $(\rho, P, \mathrm{v}_x, \mathrm{v}_y, B_y) = [1, 20, 10, 0, 5/(4\pi)^{1/2}]$ and to the right by $(\rho, P, \mathrm{v}_x, \mathrm{v}_y, B_y) = [1, 1, -10, 0, 5/(4\pi)^{1/2}]$ with $B_x = 5.0/(4\pi)^{1/2}$ and $\gamma = 5/3$. Results are shown at time $t = 0.08$ and compare well with the exact solution given by Dai and Woodward (1994) (solid line).

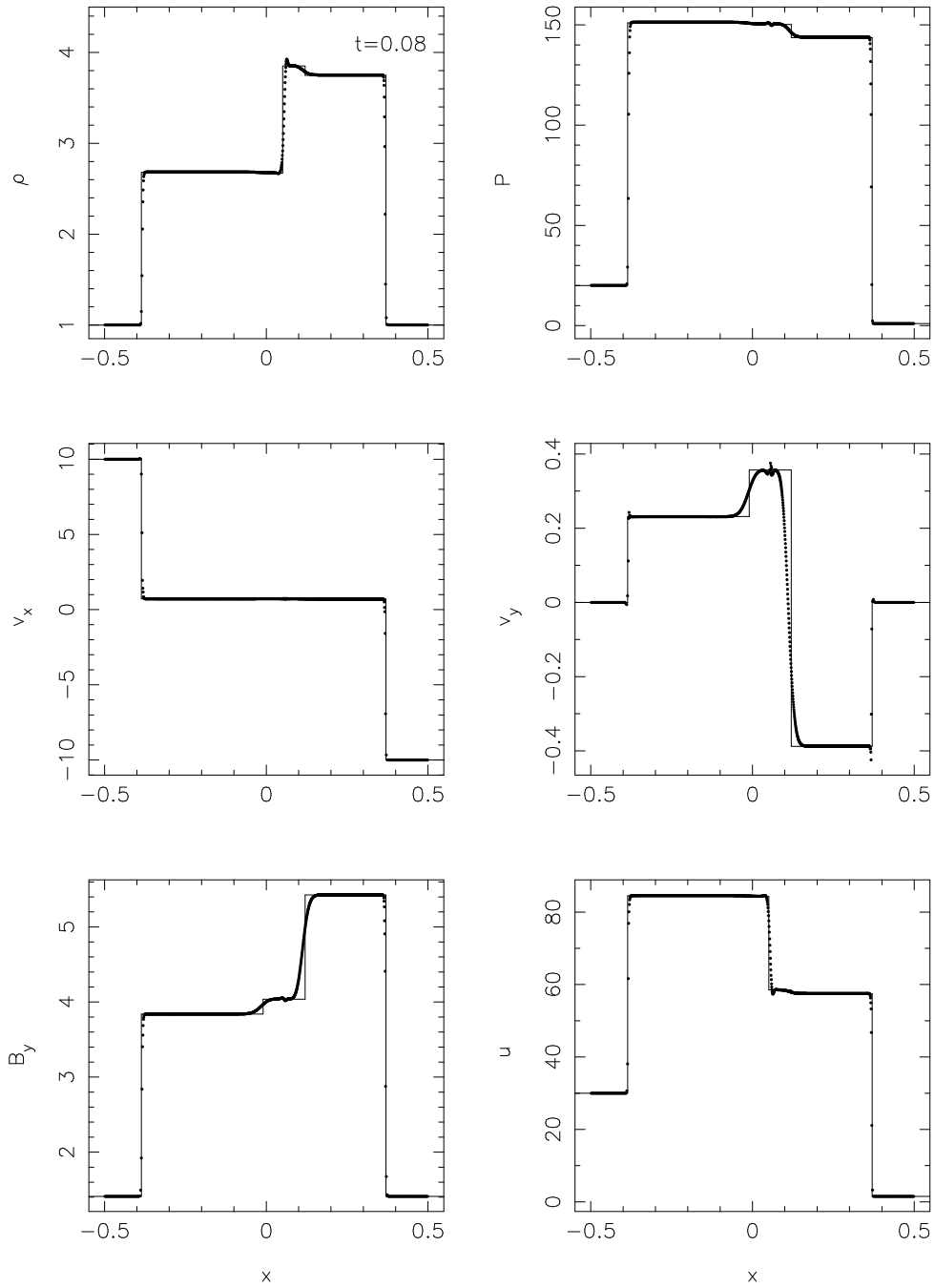

Figure 4.19: Results of the MHD shock tube test shown in Figure (4.18) with the density calculated by summation and using the variable smoothing length terms. Results compare extremely well with the exact solution (solid line). In particular the overshoots in transverse magnetic field and velocity observed in Figure 4.18 are no longer present.

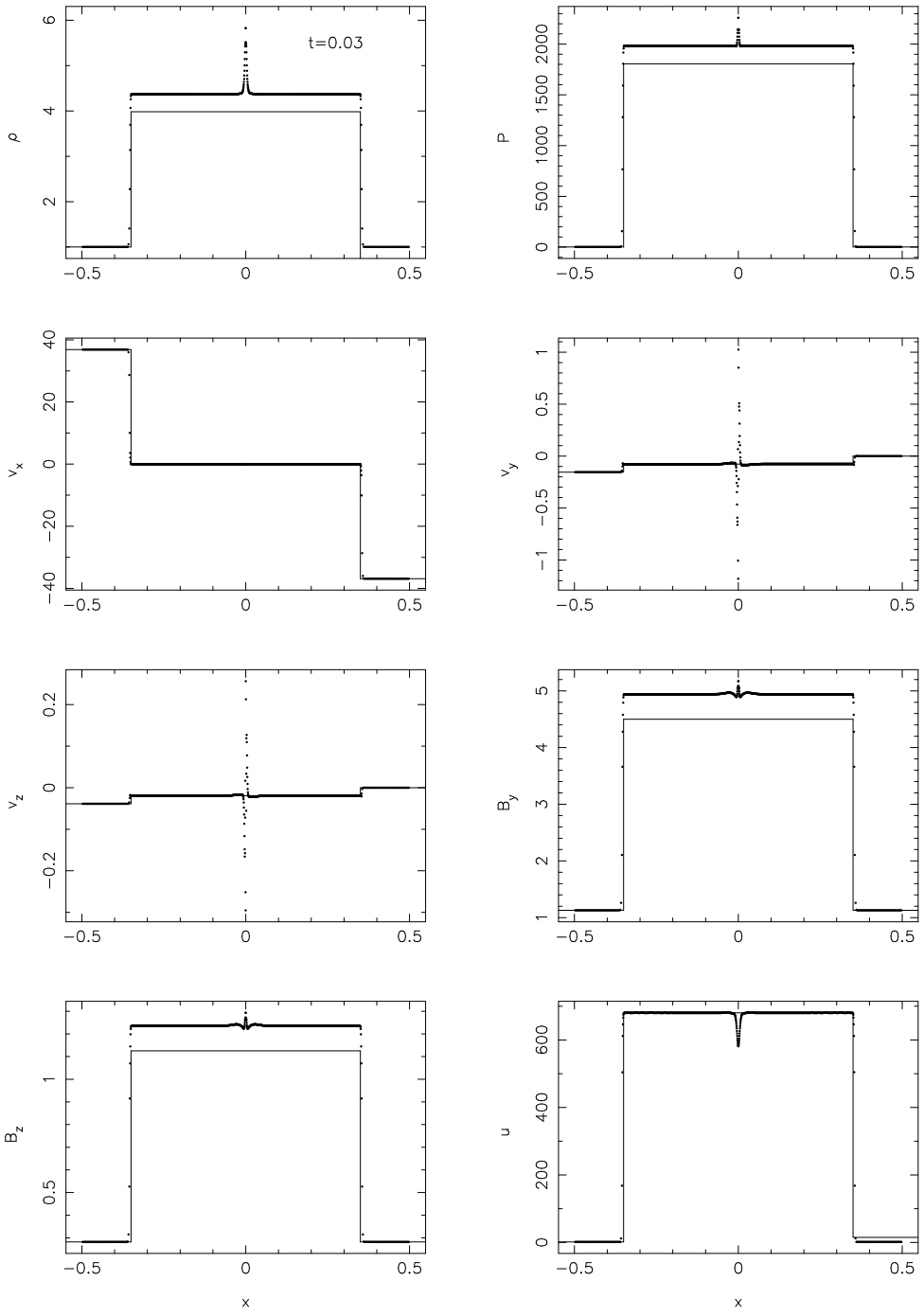

Figure 4.20: Results of the MHD shock tube test with left state $(\rho, P, \mathrm{v}_x, \mathrm{v}_y, \mathrm{v}_z, B_y, B_z) = [1, 1, 36.87, -0.155, -0.0386, 4/(4\pi)^{1/2}, 1/(4\pi)^{1/2}]$ and right state $(\rho, P, \mathrm{v}_x, \mathrm{v}_y, \mathrm{v}_z, B_y, B_z) = [1, 1, -36.87, 0, 0, 4/(4\pi)^{1/2}, 1/(4\pi)^{1/2}]$ with $B_x = 4.0/(4\pi)^{1/2}$ and $\gamma = 5/3$. Results are shown at time $t = 0.03$. This problem illustrates the formation of two extremely strong fast shocks of Mach number 25.5 each. Solid points indicate the position of the SPH particles whilst the exact solution is given by the solid line. The overshoots in density, pressure and magnetic field are a result of our integration of the continuity equation and neglect of terms relating to the gradient of the smoothing length.

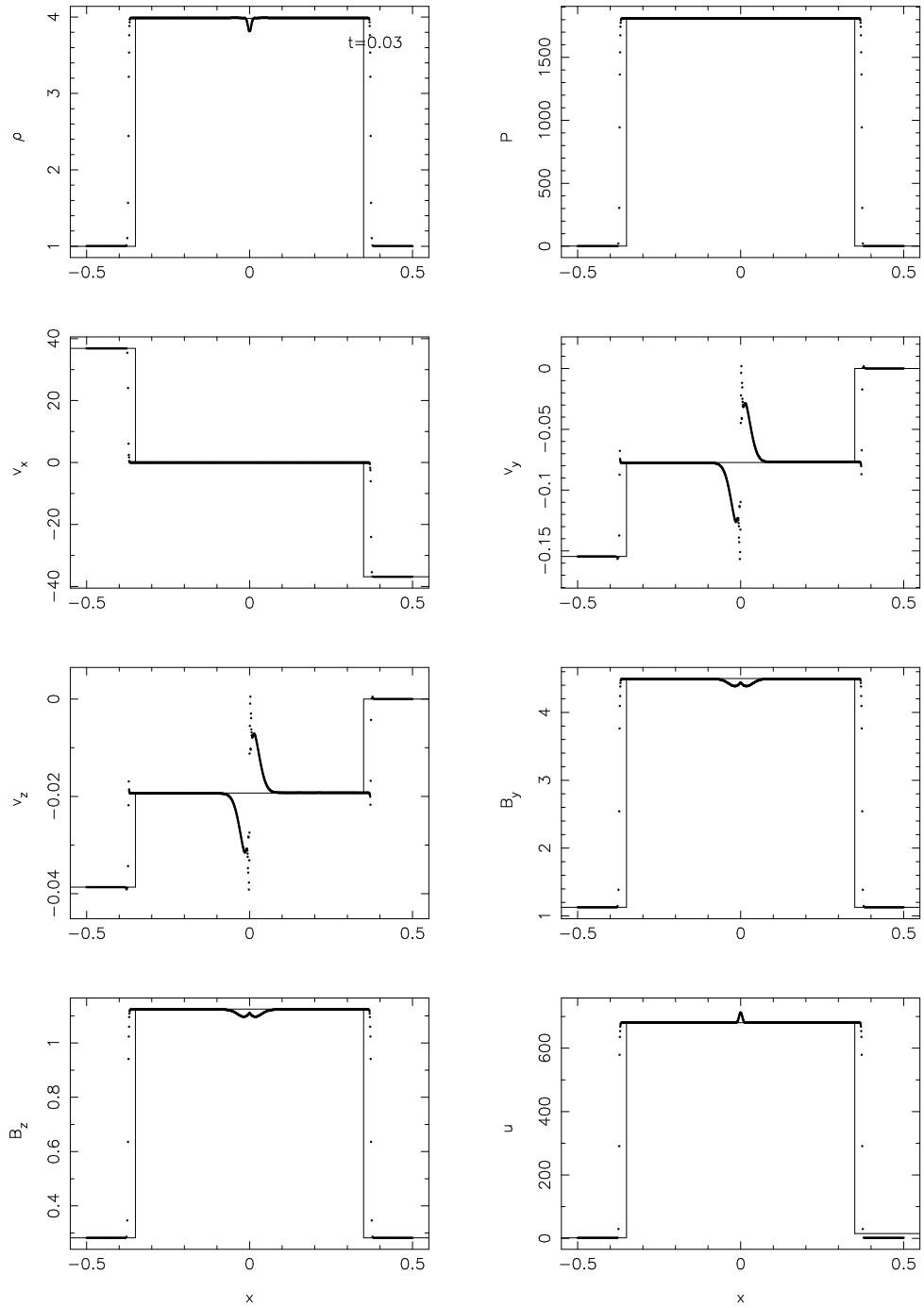

Figure 4.21: Results of the MHD shock tube test shown in Figure 4.20 with the density calculated by summation and using the variable smoothing length terms. The overshoots in density, pressure and magnetic field observed in Figure 4.20 are no longer present and the spikes in the transverse velocity components at the contact are much smaller in magnitude.

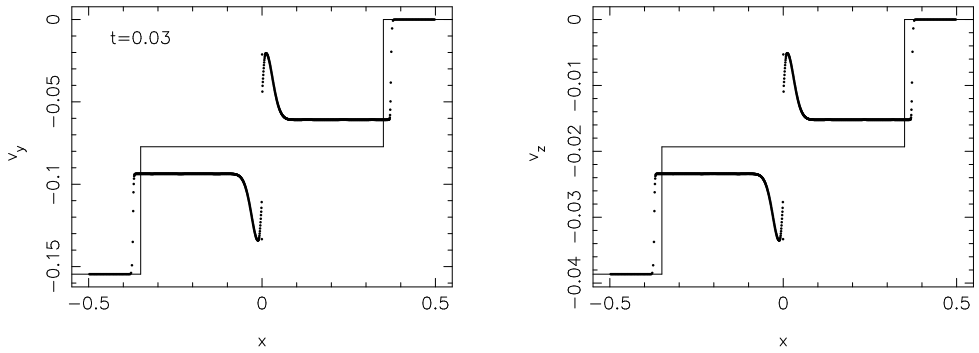

Figure 4.22: Transverse velocity profiles in the MHD shock tube test shown in Figure 4.20 using the Morris (1996) formalism (§4.4.2), also with the variable smoothing length terms. A small error in the intermediate states around the contact discontinuity is observed in this case due to the non-conservation of momentum on the anisotropic force terms. However, the error is quite small.

scheme. The left state is $(\rho, P, \mathrm{v}_x, \mathrm{v}_y, \mathrm{v}_z, B_y, B_z) = [1, 1, 36.87, -0.155, -0.0386, 4/(4\pi)^{1/2}, 1/(4\pi)^{1/2}]$ with right state $(\rho, P, \mathrm{v}_x, \mathrm{v}_y, \mathrm{v}_z, B_y, B_z) = [1, 1, -36.87, 0, 0, 4/(4\pi)^{1/2}, 1/(4\pi)^{1/2}]$ with $B_x = 4.0/(4\pi)^{1/2}$ and $\gamma = 5/3$. Results are shown in Figure 4.20 at time $t = 0.03$. Inflow boundary conditions are used such that the resolution varies from an initial 400 particles up to 1286 particles at $t = 0.03$ in the domain $x = [-0.5, 0.5]$. The results compare extremely well with the exact solution (solid line) given by Dai and Woodward (1994) and with the numerical solution given by Dai and Woodward (1994) and Balsara (1998), especially given the extreme nature of the problem. The spikes in transverse velocity components are due to the fact that firstly, no smoothing is applied to the initially discontinuous velocity profiles in this case, and secondly that these components are only implicitly smoothed in the simulation by the application of artificial resistivity to the transverse magnetic field components. The overshoots in density and pressure are absent when the density is calculated by direct summation. As in the previous test, the overshoots in magnetic fields are no longer observed when the variable smoothing length terms are included (Figure 4.21). Using the variable smoothing length terms the spikes observed in the transverse velocity components at the contact discontinuity are also much smaller. The results of this test using the Morris (1996) formalism (§4.4.2) are shown in Figure 4.22, also using the variable smoothing length terms (although the average of the normalised kernel gradients is used in the anisotropic force, as described in §4.4.2). In this case a small error in the intermediate states around the contact discontinuity is observed due to the non-conservation of momentum on the anisotropic force terms. However the error is quite small even for this somewhat extreme problem.

4.6.4 MHD waves

The usefulness of the variable smoothing length terms can also be demonstrated, as in the hydrodynamic case (3.7.2), by the simulation of linear waves. The equations of magnetohydrodynamics admit three 'families' of waves, the so called slow, Alfvén and fast waves (appendix C). The tests presented here are taken from Dai and Woodward (1998). We consider travelling slow and fast MHD waves propagating in a 1D domain, where the velocity and magnetic field are allowed to vary in three dimensions. We use $\gamma = 5/3$ for the problems considered here. The perturbation in density is applied by perturbing the particles from an initially uniform setup (since we use equal mass particles). Details of this perturbation

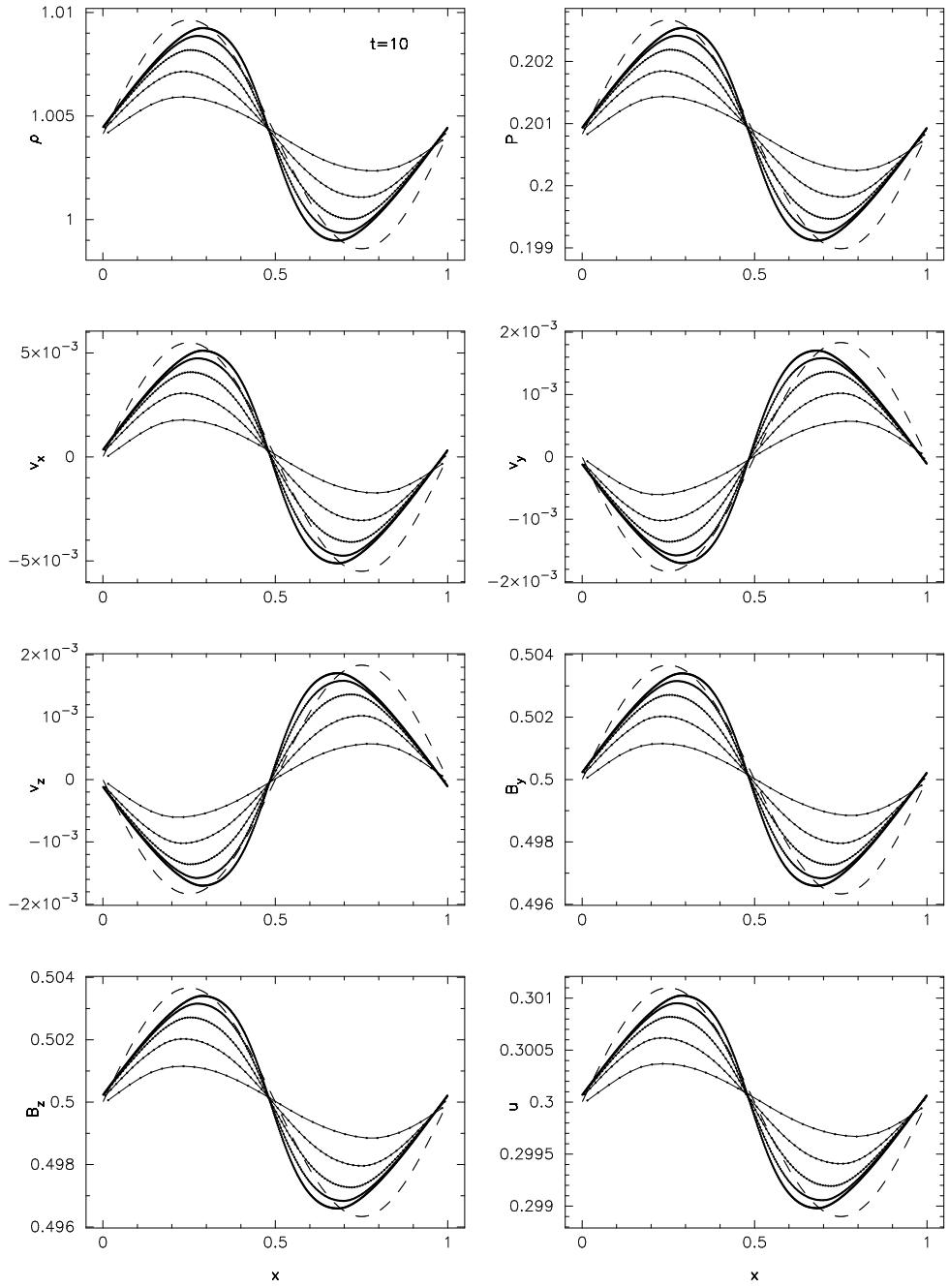

Figure 4.23: Results for the 1D travelling fast wave problem. Initial conditions are indicated by the dashed line. Results are presented after 10 periods for simulations with 32, 64, 128, 256 and 512 particles. The fast wave speed in the gas is very close to unity which is accurately reproduced by the SPMHD solution (ie. the numerical solution is in phase with the initial conditions). The artificial dissipation terms are turned on but controlled using the switches described in §3.5.2 and §4.5.2 which dramatically reduces their effects away from shocks. The wave is steepened slightly by nonlinear effects.

are given in 3.7.2 and the amplitudes for the other quantities are derived in appendix C. We leave the artificial dissipation terms on for this problem using the viscosity, thermal conductivity and resistivity switches. This is to demonstrate that the switches are effective in turning off the artificial dissipation in the absence of shocks. The variable smoothing length terms (§4.3.6) do not affect the wave profiles but inclusion of these terms gives very accurate numerical wave speeds.

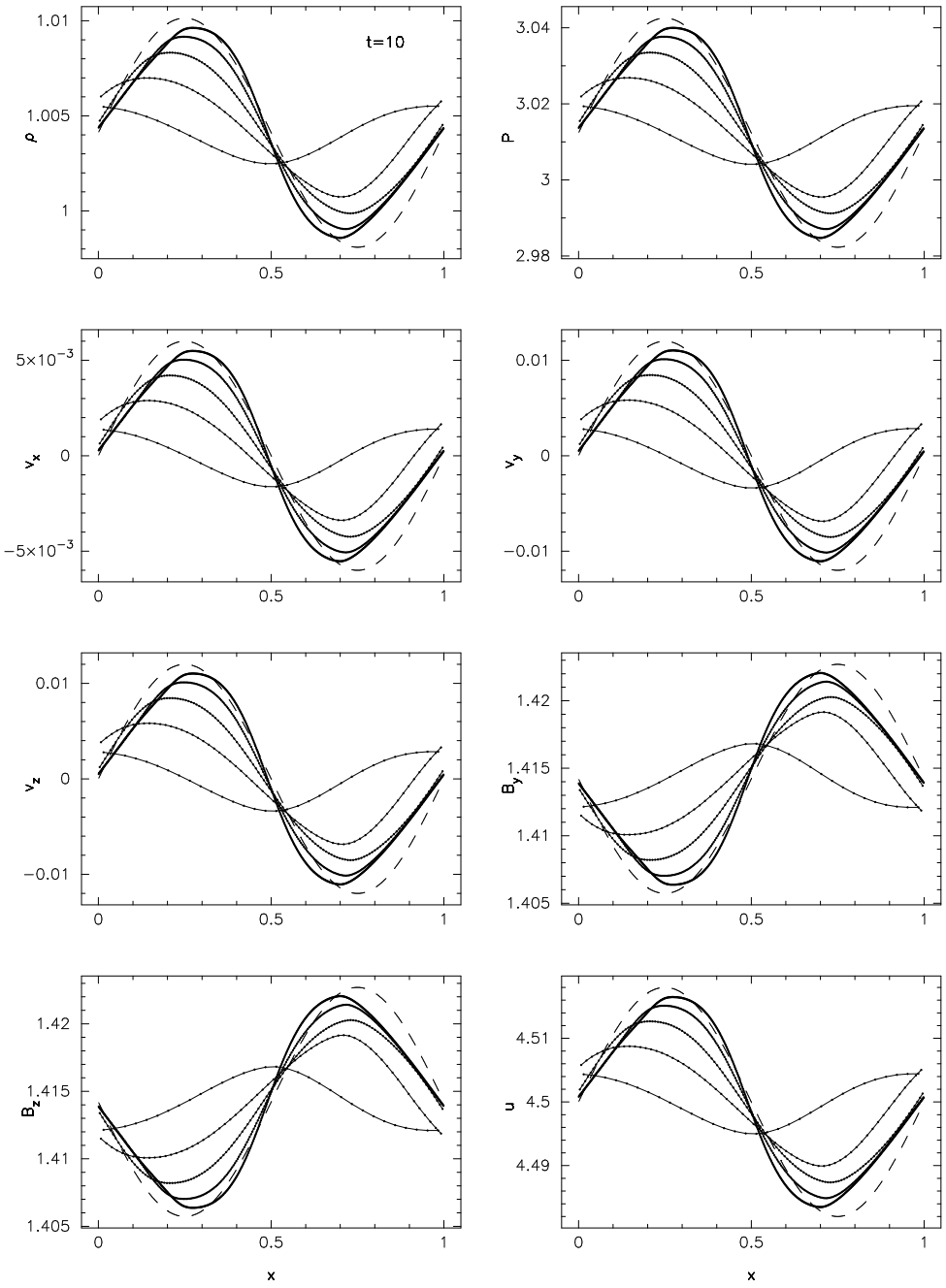

Figure 4.24: Results for the 1D travelling slow wave problem. Initial conditions are indicated by the dashed line and results are presented after 10 periods for simulations with 32, 64, 128, 256 and 512 particles. The slow wave speed in the gas is very close to unity, such that the numerical solution at $t = 10$ should be in phase with the initial conditions. This is well represented by the SPMHD solution for the higher resolution runs. The artificial dissipation terms are turned on but we have used the switches described in §3.5.2 and §4.5.2 which dramatically reduce their effects away from shocks. The wave is steepened slightly by nonlinear effects.

The fast wave is shown in Figure 4.23, with the dashed line giving the initial conditions. The initial amplitude is 0.55% as in Dai and Woodward (1998). Results are shown at t=10 for five different simulations using 32, 64, 128, 256 and 512 particles in the x-direction. The properties of the gas are set such that the fast wave speed is very close to unity, meaning that the solution at $t = 10$ should be in phase

with the initial conditions. Figure 4.23 demonstrates that this is accurately reproduced by the SPMHD algorithm. The effects of the small amount of dissipation present can be seen in the amount of damping present in the solutions. The small amount of steepening observed in the wave profiles is due to nonlinear effects and agrees with the results presented by Dai and Woodward (1998).

The slow MHD wave is shown in Figure 4.24, again with the dashed line giving the initial conditions. The perturbation amplitude is 0.6% as in Dai and Woodward (1998). Results are again shown at $t = 10$ at resolutions of 32, 64, 128, 256 and 512 particles.In this case the properties of the gas being set such that the slow wave speed in the medium is very close to unity, again meaning that the solution at $t = 10$ should be in phase with the initial conditions. We see in Figure 4.24 that this is reproduced by the SPMHD solution for the higher resolution runs. The artificial dissipation terms are again turned on using the switches. The wave is slightly overdamped in this case since we construct the artificial dissipation using the fastest wave speed (§4.5) which in this case is approximately three times the wave propagation speed. This means that the convergence of the wave amplitude towards the linear solution with increasing resolution is quite slow for this problem.

4.6.5 Magnetic toy stars

As was noted in the previous chapter, for codes designed to simulate self-gravitating gas it is useful to provide numerical benchmarks which do not involve fixed boundaries. As such a class of exact solutions to the hydrodynamic equations with a force proportional to the co-ordinates was described in §3.7.6, referred to as 'Toy Stars'. In §3.7.6 the exact solutions for the non-linear oscillations of the Toy Star was used to benchmark the purely hydrodynamic SPH algorithm.

The exact non-linear solution for the toy star described in §3.7.6 may be easily extended to the MHD case. The simplest case is to assume that the only non-zero component of the magnetic field is in the $y-$direction. In this case the induction equation (4.7) becomes

$$\frac{dB^y}{dt} = -B^y \frac{\partial \mathrm{v}^x}{\partial x} \tag{4.105}$$

which shows that $B^y \propto \rho$. The one dimensional equation of motion for the magnetic toy star therefore becomes

$$\frac{d\mathrm{v}^x}{dt} = -\frac{1}{\rho}\frac{\partial}{\partial x}\left(P + \frac{B^2}{2\mu_0}\right) - \Omega^2 x \tag{4.106}$$

where $B^2 = (B^y)^2$. By assuming the same constant of proportionality between B^y and ρ for each particle such that $B^y = \sigma\rho$, the exact solution for the MHD system is exactly the same as in the hydrodynamic case (for $\gamma = 2$), except that the constant K is replaced by

$$K' = K + \frac{\sigma^2}{2\mu_0} \tag{4.107}$$

such that the effective pressure P (including both gas and magnetic pressures) is specified according to $P = K'\rho^2$. The exact solution is then calculated by solving the ordinary differential equations (3.143)-(3.145) as described in §3.7.6.

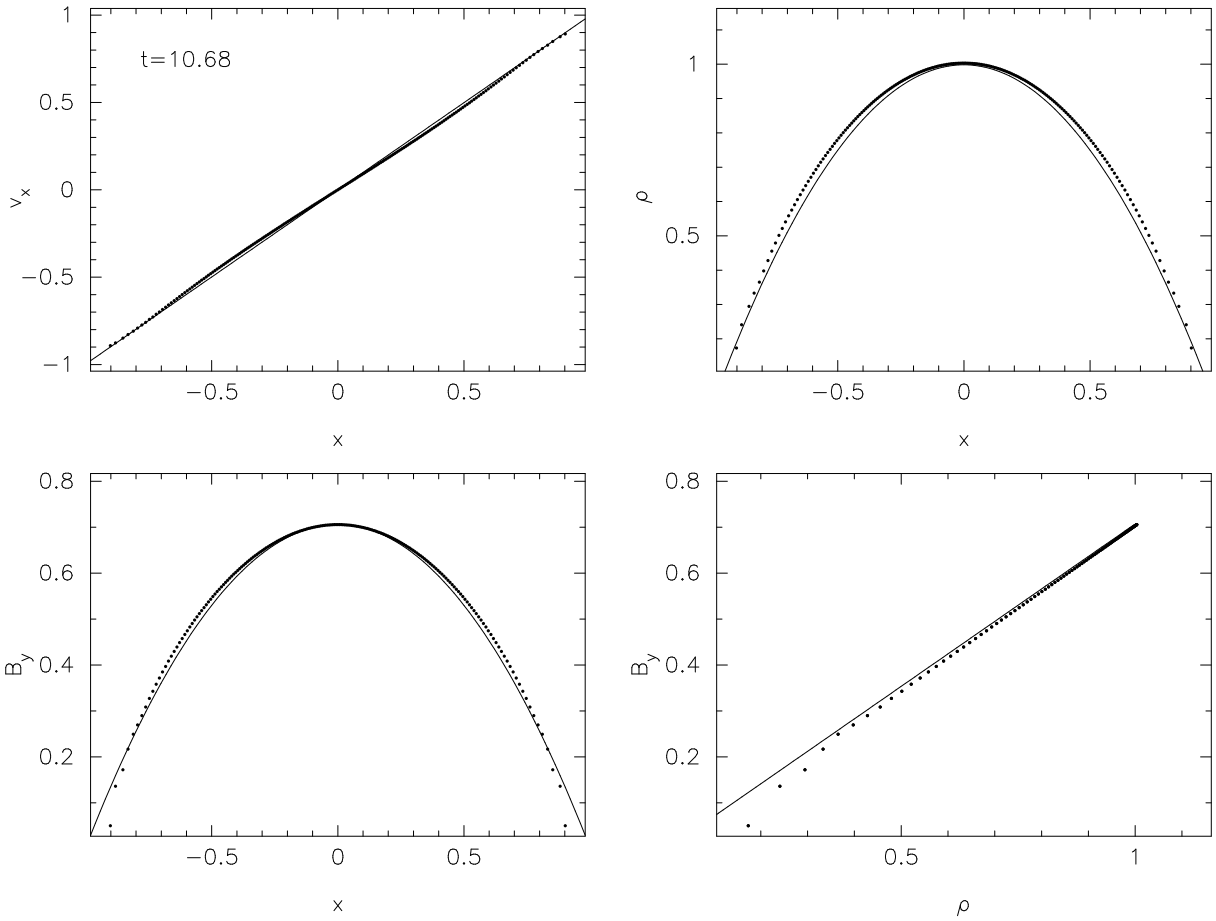

Figure 4.25: Results of the non linear, magnetic Toy star simulation with initial conditions v $= x$, $\rho = (1-x^2)$, $B^y = \rho/\sqrt{2}$ (ie. $A = C = H = 1$, $\sigma = 1/\sqrt{2}$ and $\gamma = 2$), shown after approximately three oscillation periods. Equal mass particles are used with a variable initial separation, whilst the magnetic field is chosen such that gas pressure and magnetic pressure are equal in magnitude.

For the SPMHD solution, the magnetic case the magnetic field is evolved using the SPH form of equation (4.20) with the magnetic field and velocity allowed to vary in two dimensions whilst the particles are constrained to move along the x-axis. We set $\gamma = 2$ and choose the magnetic field strength such that the ratio of gas to magnetic pressure, $\beta = 1$, ie. $\mathbf{B} = (0, 1/\sqrt{2}\rho, 0)$. For this simulation we apply a small amount of artificial viscosity using the switch in order to damp the small oscillations resulting from the rapid movement of the outer edges. Results are shown in Figure 4.25 at $t = 10.68$, corresponding to approximately three oscillation periods in this case. As in the hydrodynamic case the agreement with the exact solution (solid line) is extremely good.

4.7 Summary

In this chapter we have derived the basic formalisms necessary for the simulation of magnetic fields using the Smoothed Particle Hydrodynamics method. All of the technical difficulties described in the introductory section have been addressed to a level where quite satisfactory solutions can be obtained for many astrophysical problems, although many improvements to the algorithm could still be made. Of these the most important is to implement a cleaning procedure for the magnetic divergence and hence we

devote chapter 5 to this topic.

Reviewing this chapter, the equations of magnetohydrodynamics in the continuum limit were described in §4.2.1, paying particular attention to the consistent formulation of these equations in the presence of magnetic monopoles, since the $\nabla \cdot \mathbf{B} = 0$ constraint cannot be maintained exactly in all discretisations in any numerical scheme. Conserved quantities which can be monitored in addition to the usual hydrodynamic quantities were discussed in §4.2.2. In §4.3 SPH formulations of the MHD equations were presented. The equations of motion and energy were derived self-consistently from a variational principle using the discrete forms of the continuity and induction equations as constraints, using a form of variational principle similar to that used to derive alternative formulations of the SPH equations in §3.4. In the MHD case this was shown to remove the ambiguity over the inclusion or neglect of terms proportional to $\nabla \cdot \mathbf{B}$ in the induction and momentum equations which has been highlighted recently by several authors. The derivation showed that a monopole-conserving form of the induction equation is in fact consistent with a conservative formulation of the momentum and energy equations. Furthermore the derivation from a variational principle guarantees consistency between the discrete formulations of these equations. Consistent alternative formulations of the SPMHD equations were given in §4.3.4, similar to those derived in the SPH case (§3.4). Other formulations of the magnetic force terms which have been used for SPMHD were also discussed briefly in §4.3.5, the main disadvantage to these formalisms being the lack of momentum conservation which leads to extremely poor results on problems involving shocks. The consistent formulation of the SPMHD equations incorporating a variable smoothing length was discussed in §4.3.6, which, as in the hydrodynamic case are shown to lead to increased accuracy in a wide range of problems, including linear waves (§4.6.4) and shock tubes (§4.6.3).

A one dimensional stability analysis for the self-consistent formulation of SPMHD derived in §4.3 was presented in §4.4. This somewhat limited stability analysis was sufficient to highlight the instability in the momentum conserving form of the equations of motion which occurs at short wavelengths under negative stresses and leads to a clumping effect between particles. An approach to remove this instability was described in §4.4.1, following the ideas of Monaghan (2000) in which a fictitious short range force is added which counteracts the clumping effect. This force takes the form of an artificial stress which is proportional to the anisotropic component of the total stress, which is the interpretation given by Monaghan (2000). In §4.4.1 an alternative interpretation was given in terms of a modification to the kernel gradient used in the anisotropic force term. This interpretation considerably simplified the stability analysis including the anticlumping term presented in §4.4.1, which demonstrated that whilst (for fixed h) the term very effectively removes the instability, one disadvantage is an error in the numerical wave speed which grows with increasing negative stress. This error was shown to be reduced significantly (although not removed) by a small modification to the anticlumping term which changes the kernel shape at a fixed r/h rather than in relation to the average particle separation. However a major caveat to the anticlumping approach is that the formalism was not found to be stable for all values of negative stress in the case of a variable smoothing length. Various alternative approaches were therefore suggested. An approach which can be used in many practical situations is to simply subtract any constant component of the magnetic field from the gradient term representing the anisotropic force (§4.4.4). For situations where this cannot be used, an alternative approach suggested by Morris (1996) (§4.4.2) was found to also give good results on the shock tube tests described in §4.6.3.

In §4.5 dissipative terms were formulated in order to simulate MHD shocks. The terms are a natural

generalisation of the formalism of Monaghan (1997b) given for the hydrodynamic case in §3.5. The dissipation terms were derived under a minimum of assumptions by assuming a dissipation in the total energy equation which involves a jump in the total energy and requiring that this term result in a positive definite contribution to the entropy. Under only these two assumptions a discrete formulation for a dissipative term in the induction equation was obtained which involves the SPH formulations of the second derivative given in §3.2.4. This term was shown to provide an artificial resistivity in addition to the artificial viscosity and artificial thermal conductivity derived in the hydrodynamic case. A slightly modified version of these dissipative terms which accounts for jumps in the component of the magnetic field along the line joining the particles (due to non-zero magnetic divergence) and velocities perpendicular to this line (providing a shear viscosity component) was also presented. A switch to control the application of artificial resistivity was given in §4.5.2, although it was noted that in the absence of a shear viscosity term it is better to apply artificial resistivity uniformly so as to provide sufficient smoothing of the discontinuities in both the magnetic field and transverse velocity.

Finally, detailed one dimensional numerical tests were presented in §4.6. In particular the algorithm has been tested on a wide range of standard test problems used to benchmark recent grid-based MHD codes. A simple advection test was first considered (§4.6.2), before considering a wide range of shock tube problems demonstrating the shock-capturing ability of the algorithm (§4.6.3). In particular the shock tube tests highlighted the fact that artificial resistivity is a crucial requirement in order to prevent post-shock oscillations in the magnetic field. For high Mach number shocks, the density (although only where the continuity equation is integrated) and magnetic field are observed to overshoot the exact solution slightly, although this error is removed by the inclusion of the variable smoothing length terms which provide a normalisation to the kernel gradient. The algorithm was also tested against small amplitude both fast and slow MHD waves (§4.6.4) and shown to give good results although somewhat slow convergence on these problems due to the dissipative terms.